

## **Nuclear Transmutations in Critical and Supra-critical Electrolysis with Graphite, Pd, W, Re, Pt and Au Cathodes Analyzed by the TNCF Model**

Hideo Kozima, Tadayoshi Ohmori\*and Masayuki Ohta,

Cold Fusion Research Laboratory

<http://www.geocities.jp/hjrfq930/>

597-16 Yatsu, Aoi, Shizuoka, 421-1202 Japan

\*Advanced Technology, Inc., Hokkaido Institute of Technology,

7-15 Maeda, Teine, Sapporo, 006-8585 Japan

### **Abstract**

Nuclear transmutations observed in the surface region of cathodes made of C (graphite), Pd and 5d elements (W, Re and Au) used in normal, critical and supra-critical electrolysis with light water in addition to some data observed with heavy water are analyzed using the trapped neutron catalyzed fusion (TNCF) model. The occurrence of the cold fusion phenomenon in 5d transition-metal electrodes is consistently explained in accordance with the cold fusion phenomenon (CFP) observed in 3d and 4d transition-metal hydrides and deuterides, such as  $NiH_x$  and  $PdD_x$ , at the normal electrolysis. The necessary conditions for the realization of the CFP, formation of super-lattice of host nuclei and protons/deuterons in these hydrogen non-occluding materials (at near room temperature) are realized by the higher temperatures of the material induced by a long electrolysis at normal electrolysis (up to three weeks) or by the critical and supra-critical electrolysis with high current densities. Using the data analyzed in this paper in addition to the data obtained in 3d and 4d transition-metals analyzed hitherto, we could contemplate some characteristics of the CF-matter responsible for the nuclear transmutations in the CFP.

**Key words**; nuclear transmutation, cold fusion phenomenon, critical electrolysis, glow discharge, arc discharge, TNCF model,

### **1. Introduction**

The cold fusion phenomenon (CFP) composed of various events, including nuclear transmutation, emission of neutrons with energies from 2.5 up to 20 MeV, generation of tritium and large excess heat, has been observed for more than 25 years mainly in 3d and 4d transition-metal hydrides and deuterides such as  $NiH_x$  and  $PdD_x$  [Kozima 1998,

2006] besides in XLPE [Kozima 2016c] and biological cultures [Kozima 2016d]. The experimental data sets with large dispersion in the CFP have been successfully analyzed phenomenologically using a model (the trapped neutron catalyzed fusion (TNCF) model) proposed in 1993 at ICCF4 [Kozima 1994] in consistency with knowledge of modern physics. The basic assumptions of the model, especially the existence of the trapped neutrons in materials (CF materials) where the CFP was observed have been explained using the novel knowledge of solid-state physics and nuclear physics [Kozima 2006, 2016c].

It should be remembered that the idea of the neutron energy band introduced in the process of the justification of the trapped neutrons in the CF materials may have close relations with such physical characteristics of the transition-metal hydrides and deuterides as extraordinary large diffusivity of H and D in them. Anyway, the novel knowledge of the interaction among lattice nuclei mediated by occluded H or D disclosed by the CFP will open a new perspective of solid state-nuclear physics in these materials.

In relation to the CFP, there are several modes of electrolysis to charge hydrogen isotopes into metals; the most popular one is the electrolysis of light and heavy waters with alkaline ions in electrolytic liquids at a relatively low current density (let us call this case the normal electrolysis) to charge hydrogen isotopes into CF materials (hydrogen occluding metals) such as Ni, Ti and Pd (e.g. [Fleischmann 1989, McKubre 1991]). We have analyzed mainly these data sets of the normal electrolysis hitherto [Kozima 1998, 2006]. There are other types of electrolysis with higher current densities; one is the arc discharge between carbon (graphite) rods in water (e.g. [Hanawa 2000]) successfully analyzed before [Kozima 2012]. This stage of current flow between two electrodes is called “the supra-critical electrolysis” hereafter together with another stage of electrolysis explained below.

Another mode of electrolysis left aside until now is “the critical electrolysis” [Ohmori 2016] taken up in this paper.

To make our image of electrolysis clear, we cite here the case of electrolysis with palladium cathodes with varying current density. The critical electrolysis occurs in the case of Pd cathodes as follows:

Let us consider the experiment performed by the current control scheme. When the current density  $i$  is less than a critical value  $i_0$ , the electrolysis is in a steady state. However, when the current density exceeds  $i_0$ , the electrode potential suddenly becomes unstable. We call the electrolysis at the current density  $i_0$  “the critical electrolysis” ([Ohmori 2002, 2004]) and the electrolysis with a current density  $i \geq i_0$  is called “the

supra-critical electrolysis” in this paper for convenience of discussion. In the supra-critical electrolysis, at 5 – 10 minutes after arriving at the critical condition, the glow discharge occurs (called also as “the plasma electrolysis” [Ohmori 1998c]), and the electrode becomes incandescent.

As soon as the electrolysis reaches at the critical condition, the regulated DC current-control mode of power supply changes instantaneously to the potential-control mode owing to the momentary jump of the electric resistance of the electrode/solution interface.

### **Classification of Electrolysis according to Cathode Phenomena**

In summary, we can classify the electrolysis according to the current density at the cathodes, i.e. according to the cathode temperature which affects the behavior of H and D at the cathode.

The electrolysis is classified in three types according to the current density  $i$ ;

(1) Normal electrolysis; current density  $i \leq \sim 1 \text{ A/cm}^2$ ,

(2) Critical electrolysis; current density in between 1 and 5  $\text{A/cm}^2$ ;  $\sim 1 \text{ A/cm}^2 \leq i \leq \sim 5 \text{ A/cm}^2$ ,

and

(3) Supra-critical electrolysis; current density  $i > 5 \text{ A/cm}^2$ .

In the supra-critical electrolysis, there occurs glow or arc discharge.

We can cite several examples of these electrolysis from the history of the CF research as follows;

**Normal electrolysis;** [Fleischmann 1989]  $i < 512 \text{ mA/cm}^2$ , [McKubre 1991] (typically  $i = 300\text{-}600 \text{ mA/cm}^2$ , but up to  $6400 \text{ mA/cm}^2$ ), [Silver 1993] ( $i = 250 \text{ mA/cm}^2$ ) [Dash 1994] ( $\text{H}_2\text{O} + \text{H}_2\text{SO}_4$ ,  $i = 670 \text{ mA/cm}^2$ ), [Ohmori 1998b] ( $i = 100 \text{ mA/cm}^2$ ).

**Critical electrolysis;** [Ohmori 1998, 2002, 2004, 2016]  $i \sim 3.13 - 3.75 \text{ A/cm}^2$ , [Ohmori 2002, 2004 (Pd)]

**Supra-critical electrolysis;** [Ohmori 1999, Mizuno 1998a, Hanawa 2000] glow discharge or plasma electrolysis and arc discharge at higher voltages (up to 240 V)., [Ohmori 1999] (W)  $i \sim 2.5\text{A}/0.5\text{cm}^2 = 5 \text{ A/cm}^2$ . [Hanawa 2000] graphite rods electrodes  $\phi = 6 \text{ mm}$ ,  $I = 30 \text{ A}$ ,  $i \sim 100 \text{ A/cm}^2$ ,  $V = 20 \text{ V}$  and  $Q_{\text{in}} = 600 \text{ W}$ ).

### **Some characteristics of electrodes in these electrolysis conditions;**

(1) In the “Normal Electrolysis,” the cathode temperature is in equilibrium with the surrounding electrolyte, and does not become higher than  $100 \text{ }^\circ\text{C}$  (or the boiling point of the electrolytic liquid).

- (2) In the “Critical Electrolysis,” the cathode is heated by the proton or deuteron current absorbed by the cathode (Especially, in the case of Pd, the process is exothermic.).
- (3) In the “Supra-critical Electrolysis,” the process becomes glow or arc discharge in the liquid, and the cathode is heated more than that in the critical electrolysis up to the boiling point of the electrolytic liquid. In the arc, the anode is also heated very high up to about 3000 K [Hanawa 2000].

In this paper, we take up mainly experimental data sets obtained with the critical and supra-critical electrolysis by Ohmori et al. and also related data sets to them to discuss the cold fusion phenomenon from the unified point of view using the TNCF model based on the solid-state nuclear physics of neutrons in CF materials.

In Section 2, we explain experimental data sets obtained in experimental systems with cathodes of graphite, Pd and 5d transition-metals. In Section 3, we summarize the essence of the TNCF model. In Section 4, we give analysis of the experimental data sets explained in Section 2 by the TNCF model.

In Section 5, we explain the meaning of the phenomenological model based on the experimental data.

In Appendices, we give a summary of physical properties of hydrogen isotopes in metals in Appendix A and the super p-p interaction between protons in interstices in solid state physics, a counterpart of the super-nuclear interaction, in Appendix B.

## **2. Experimental Data Sets on the Nuclear Transmutation in Cathodes at the Normal, Critical and Supra-critical Electrolysis with Graphite, Pd, W, Re and Au Cathodes**

The cold fusion phenomenon (CFP) has been investigated mainly in transition-metal hydrides and deuterides since the discovery of this phenomenon in a Pd/D<sub>2</sub>O+LiOD/Pt system by Fleischmann et al. in 1989 [Fleischmann 1989]. There have been investigated the CFP not only in deuterium systems (e.g. PdD<sub>x</sub> and TiD<sub>x</sub>) but also in protium systems such as NiH<sub>x</sub> and PdH<sub>x</sub> in several years after the discovery (cf. e.g. [Kozima 1998, 2006]). Thus, the CF materials where the CFP has been observed increased from the transition-metal deuterides to the transition-metal hydrides in a few years after the announcement of the CFP by Fleischmann et al.

One of the astonishing discoveries of the CFP was that there are observed nuclear transmutations, production of heavy elements, especially a large amount of iron in an unexpected CF material, graphite [Sundaresan 1994, Singh 1994, Hanawa 2000].

Another remarkable data on nuclear transmutation and excess heat have been

observed in 5d transition-metal hydrides by Ohmori et al. after 1996 which are the main subject of the analysis in this paper. The experimental data of these works are tabulated in Table 2.1, and discussed further in the following subsections.

Table 2.1 Nuclear transmutations observed in the surface region of cathodes at the critical and supra-critical electrolysis with Graphite, W, Re, Pt and Au cathodes

<b>Cathode/Electrolytic Liquid/Anode</b>	<b>Electrolysis; Normal Critical Supra-critical (SC)</b>	<b>Current density at cathode, (duration experiment)</b>	<b>Transmuted nuclei of (References)</b>
Graphite/H <sub>2</sub> O/Graphite	SC(Arc discharge in H <sub>2</sub> O)	100 A/cm <sup>2</sup> ,	Fe + Cr, Mn, Co, Ni, Cu and Zn (1)
Pd/D <sub>2</sub> O +K <sub>2</sub> CO <sub>3</sub> /Pt	N C	0.2 – 0.8 A/cm <sup>2</sup> , 3.1 – 3.8 A/cm <sup>2</sup>	Cr, Fe, Cu, Pb (5) Pd, Au, Hg, Pb(6)
Pd/H <sub>2</sub> O + Na <sub>2</sub> SO <sub>4</sub> /Pt			
W/H <sub>2</sub> O+Na <sub>2</sub> SO <sub>4</sub> + Na <sub>2</sub> CO <sub>3</sub> +K <sub>2</sub> CO <sub>3</sub> +/Pt	SC	5 A/cm <sup>2</sup> ,	Cr, Fe, Ni, Re(2,3)
Re/H <sub>2</sub> O+Na <sub>2</sub> SO <sub>4</sub> + K <sub>2</sub> SO <sub>4</sub> +K <sub>2</sub> CO <sub>3</sub> +/Pt	SC (glow discharge in H <sub>2</sub> O)	3 A/cm <sup>2</sup> ?	Fe, Cu, Zn (3)
Au/H <sub>2</sub> O+Na <sub>2</sub> SO <sub>4</sub> + K <sub>2</sub> SO <sub>4</sub> +K <sub>2</sub> CO <sub>3</sub> /Pt	N	0.2 ~ 1.5 A/cm <sup>2</sup> , (7 – 30 days)	F, Si, Fe, Pt, Hg (4)

References: (1) [Hanawa 2000], (2) [Ohmori 1999, 2000b], (3) [Ohmori 2000a], (4) [Ohmori 1996a, 1996b, 1996c, 1997a, 1997b, 1998a], (5) [Mizuno 1998, Ohmori 1998b], (6) [Ohmori 1996a, 1998b, 2002, 2004]. Detailed explanations are given below in this section.

The working conditions for “critical” and “supra-critical” electrolysis for the CFP in these 5d-transition metals are explained in the beginning of Sec. 2.1.

### **Classification of the nuclear transmutations**

The nuclear transmutations (NTs) observed in the CFP could be classified by the mechanism to generate new elements according to the TNCF model. The NTs are divided into two types, NT of the first kind (NT I) and that of the second kind (NT II). NT of the first kind (NT I) is characterized by the reaction to generate new nuclides where participates only a single neutron, and we have been able to explain experimental

data sets of this type quantitatively as shown in our papers and books [Kozima 1998, 2006, 2014a]. On the other hand, the NT of the second kind (NT II) needs neutron drops,  ${}^A_Z\Delta$  composed of  $Z$  protons and  $(A - Z)$  neutrons (cf. Sec. 3.1), to explain the data showing large changes of the proton  $Z$  and nucleon  $A$  numbers from pre-existed nuclides to new-born nuclides.

The existence of trapped neutrons in CF materials was an a priori assumption in the early stage of the TNCF model, but has been later explained by the formation of the CF-matter due to the neutron energy band realized by the super-nuclear interaction between neutrons in lattice nuclei mediated by interstitial protons or deuterons. [Kozima 2006] The CF-matter has now to be classified into type-I and type-II corresponding to the classification of the nuclear transmutation into NT I and NT II as explained in Sections 3 and 4.

## **2.1 Explanations of Data Sets of the Nuclear Transmutation by the Normal, Critical and Supra-critical Electrolysis on Graphite, Palladium and 5d Metal Electrodes**

It is interesting to notice that such materials as graphite and 5d metals with d-electrons more than 4 (W, Re, - - -) are different from hydrogen-occluding 3d and 4d metals in their interaction with hydrogen isotopes. Usually at near room temperature, the former metals are inactive to hydrogen isotopes with large positive heat of solutions as shown in Fig. A1 (Appendix A). Therefore, they usually have not been used as CF materials where is observed the cold fusion phenomenon (CFP).

The situation changes very much, if these materials are heated to higher temperatures where hydrogen isotopes tend to be absorbed and occluded. These materials at higher temperatures have similar properties to the 3d- and 4d-transition metal hydrides. The experiments performed mainly by Ohmori et al. have shown that 5d-transition metals exhibit an interesting characteristic of CF materials common to 3d- and 4d-transition metals in terms of the CFP. This characteristic is valuable not only from scientific but also from technological point of view as shown in this paper.

In the experiments with 5d transition metal electrodes, the electric power was supplied by either of the regulated DC current/voltage supplies with 160 V or 240 V maximum output potential in the case of W/H<sub>2</sub>O/Pt system. When the electrolysis is performed at current-control mode with a definite current of  $i_0$ , the electrolysis is kept normal at voltages lower than a value  $v_c$ . When the voltage exceeds a critical voltage  $v_c$  (critical electrolysis), it becomes uncontrollable, fluctuating up and down. This stage is called the “supra-critical electrolysis.” Under this situation the electrolytic solution is

heated vigorously, and, as a result, a glow discharge starts (plasma electrolysis). In the case of carbon electrode, arc discharge starts.

### 2.1.1 Hydrogen-graphite system; Graphite/H<sub>2</sub>O/Graphite

In the experiments by Sundaresan et al. [Sundaresan 1994] and by Hanawa [Hanawa 2000], a lot of iron is produced in addition to other elements such as Ca, Si, Cr, Mn, Co, Ni, Cu and Zn when carbon (graphite) is used as electrodes for arcing in water and in air. Furthermore, it is shown that the isotopic ratio of the generated iron is the same to the natural one. These data sets was analyzed by the TNCF model, and given a consistent explanation for the transmuted nuclei as a result of nuclear interactions between trapped neutrons and cathode materials [Kozima 2012].

### 2.1.2 Palladium cathode systems; Pd/D<sub>2</sub>O/Pt and Pd/H<sub>2</sub>O/Pt

Using Pd cathodes with heavy and light waters, Ohmori and his collaborators discovered nuclear transmutations of elements at surface regions of cathodes with normal and supra-critical electrolysis.

#### 2.1.2a Pd/D<sub>2</sub>O/Pt

Experiments were performed in the system of Pd/D<sub>2</sub>O+Li<sub>2</sub>CO<sub>3</sub>/Pt with current densities of 0.2 – 0.8 A/cm<sup>2</sup> [Mizuno 1998]. In the surface layer of depth about 10,000 Å, there appeared many new elements especially Ti, Cr, Fe, Cu, Sn and Pb with larger amounts compared with others. Furthermore, the isotopic abundances of chromium <sup>A</sup><sub>24</sub>Cr differed from the natural abundances as shown in Table 2.2;

Table 2.2 Isotopic changes of chromium isotopes <sup>A</sup><sub>24</sub>Cr found in the surface layer of the Pd cathode from natural ones [Mizuno 1998].

A	50	52	53	54
Natural abundance (%)	4.3	84	9.5	2.4
Measured abundance (%)	14	51	2.4	11

This experimental data is discussed in Sec. 4.2.2.

#### 2.1.2b Pd/H<sub>2</sub>O/Pt

Ohmori et al. have performed extensive measurements of the CFP in Pd/H<sub>2</sub>O+Na<sub>2</sub>SO<sub>4</sub>/Pt systems at the supra-critical electrolysis condition for a long period of time [Ohmori 1996a, 1998b, 2002, 2004]. Details of the experiments are given below, and their analysis is given in Sec. 4.2.2.

### **2.1.2b-1 Electrolysis**

#### **Electrolysis condition**

When the experiment was performed at a current density of  $2 \text{ A/cm}^2$ , the solution temperature reached ca  $60\text{-}70^\circ\text{C}$ .

When the current density was set at  $3 \text{ A/cm}^2$ , the temperature was further raised to ca.  $85^\circ\text{C}$ . Under this condition the electrode potential began to fluctuate up and down like a wave (this stage of electrolysis is termed “supra-critical electrolysis” [Ohmori 2002, 2004]), and after 5-10 minutes there occurred a glow discharge, and the electrode became in an incandescent condition. This state of electrolysis is called “plasma electrolysis.” [Ohmori 1998c]

When the electrolysis became plasma electrolysis condition, the electrolytic solution started to boil vigorously. As soon as the electrode reached plasma electrolysis condition, the regulated DC current-potential supply mode changed instantaneously from the current-control mode to the potential-control mode owing to the momentary jump of the electric resistance of the electrode/solution interface.

### **2.1.2b-2 Result**

#### **(a) Isotope distribution**

Isotopic distribution of Pd on the surface of the eight kinds of electrodes after the supra-critical electrolysis is shown in a figure [Ohmori 2016 (Fig.4)]. Without exception the isotopic abundance of the palladium electrodes deviates markedly from its natural one for all of the electrodes. In this case, there are following characteristics in common: (i) Content of  $^{108}\text{Pd}$  exceeds significantly its natural isotopic abundance for all of the electrodes: (ii) Content of  $^{110}\text{Pd}$  exceeds its natural isotopic abundance in most cases, (iii) In contrast, content of other lighter palladium isotopes are mostly below their natural isotopic abundance. Consequently, it appears that the content of heavier palladium isotopes tends to increase, whereas, the content of lighter ones tends to decrease.

#### **(b) Foreign elements**

Foreign elements with larger atomic numbers by 2 – 4, Cd and Sn, were detected after the supra-electrolysis of Pd electrode [Ohmori 2016 (Fig.7)]. The isotopic distribution of Cd is very different from its natural isotopic abundance. In this case,  $^{114}\text{Cd}$  (main isotopic component in natural Cd) was not contained in Cd detected after the electrolysis [Ohmori 2016 (Fig. 12)]. Unfortunately, isotopic distribution of Sn could not be analyzed because of overlapping of its SIMS signals with those of other

materials.

Foreign elements Pt and Au with larger atomic numbers, other than Cd and Sn, were also detected. These elements have different isotopic distributions from their natural ones [Ohmori 2016 (Fig.9)]. In this electrolysis system Pt net was used as a counter electrode. So the Pt was considered to be produced as a result of the electrodeposition of Pt dissolved from the counter electrode. The production of Au may result from the Pt similarly to the production of Cd or Sn from Pd.

### **2.1.3 Tungsten cathode system; W/H<sub>2</sub>O+Na<sub>2</sub>SO<sub>4</sub>+Na<sub>2</sub>CO<sub>3</sub>+K<sub>2</sub>CO<sub>3</sub>/Pt**

[Ohmori 1998c, 1999, 2000a, 2000b]

Information of the electrode surface after the plasma electrolysis was obtained only when W and Re electrodes with high melting point were used.

A typical example of the W electrode after the plasma electrolysis is shown in the figure [Ohmori 2016 (Fig.22)]. Foreign elements Fe, Cr, Re, Pb were detected in this case. However, the departure of isotopic abundance of Fe and Cr in this case was not so remarkable. Notable deviation of isotopic abundance is observed for Re and Pb [Ohmori 2016 (Fig. 22 and Table 7)].

### **2.1.4 Rhenium cathode system; Re/H<sub>2</sub>O+Na<sub>2</sub>SO<sub>4</sub>+K<sub>2</sub>SO<sub>4</sub>+K<sub>2</sub>CO<sub>3</sub>/Pt**

[Ohmori 2000a]

The rhenium electrode was a square foil (0.8 cm<sup>2</sup> apparent area, 0.02 cm thick). The counter electrode was a platinum net (1 cm × 10 cm, 80 mesh). The surface of the working electrode was scraped elaborately with a cleaned glass fragment to make a crystal lattice strain. The electrolysis was performed in the light water solutions of K<sub>2</sub>CO<sub>3</sub>, KNO<sub>3</sub>, Na<sub>2</sub>CO<sub>3</sub>, Na<sub>2</sub>SO<sub>4</sub>, NaNO<sub>3</sub>, NaClO<sub>4</sub>, Rb<sub>2</sub>CO<sub>3</sub>, Ba(ClO<sub>4</sub>)<sub>2</sub>, and Ba(NO<sub>3</sub>)<sub>2</sub>.

The condition of the glow discharge can be accomplished as follows; first, pre-electrolysis was conducted galvanostatically at a current density of 2 A/cm<sup>2</sup> for 1 – 1.5 hours by which hydrogen was loaded in the electrode. Then the current density was increased step-wisely for ca. 30 minutes. When the current density exceeds ca. 3 A/cm<sup>2</sup>, the applied potential turned labile, and, after the passage of several minutes, the electrode incandescenced, and emitted red-violet glow.

When the experimental condition reaches glow discharge, the electric power source operating in the galvanostatic mode switches automatically to the potentiostatic mode owing to the rapid increase in the electric resistance at the electrode/solution interface. As a result, the input potential jumped up to 160 V, and the current density dropped down to 0.8 – 1 A/cm<sup>2</sup>, and thereafter gradually decreased, as a whole, down to ca. 0.5

A/cm<sup>2</sup>.

After the supra-critical electrolysis with a glow discharge, Fe, Cu and trace amount of Zn or only Zn was detected in the Re electrodes at surface layers of widths about 100 Å. The data of transmutation observed in the Re electrodes are discussed in Sec. 4.

#### 2.1.5 Gold cathode system; Au/H<sub>2</sub>O+Na<sub>2</sub>SO<sub>4</sub>+K<sub>2</sub>SO<sub>4</sub>+K<sub>2</sub>CO<sub>3</sub>/Pt [Ohmori 1997b]

Experiments of the normal electrolysis on the hydrogen non-occluding gold cathodes have been performed on Au cathodes with approximate dimensions of 1.0, 2.5 and 5.0 cm<sup>2</sup> × 0.1 mm in electrolytic liquids (H<sub>2</sub>O + Na<sub>2</sub>SO<sub>4</sub> (K<sub>2</sub>SO<sub>4</sub>, K<sub>2</sub>CO<sub>3</sub>)) for fairly long time-duration of 7 – 30 days with electrolytic current densities of 0.1 – 1.0 A/cm<sup>2</sup>. The experiments with Au cathode for fairly long times (up to 30 days) and higher current densities up to 1 A/cm<sup>2</sup> in normal electrolysis scheme have revealed several interesting features of the CFP in electrolytic systems as discussed in Sec. 4.

Details of experimental data in this system are introduced in Sec. 2.3

### 2.2 Critical Electrolysis with Palladium Cathode-Light Water system;

Pd/D<sub>2</sub>O+K<sub>2</sub>CO<sub>3</sub>/Pt and Pd/H<sub>2</sub>O+ Na<sub>2</sub>SO<sub>4</sub>/Pt

Palladium, a hydrogen occluding metal, is the first metal used for the CF material due to its large content of hydrogen at near room temperature (e.g. [Fleischmann 1989, McKubre 1993]). The characteristics of hydrogen isotope-palladium system are peculiar at its inverse-mass dependence of diffusivity and other properties of protium and deuterium. Below about 200 °C, deuteron is more diffusive than proton in Pd. As a result, the Pd-D system is appropriate to measure the cold fusion phenomenon (CFP) than the Pd-H system, even if protium is occluded in palladium (cf. Fig. A3 in Appendix). Above about 200 °C, the diffusivity of proton and deuteron becomes normal, i.e. the former has larger diffusivity than the latter. This is the reason that the critical electrolysis for the Pd + H system is appropriate for the CF research as successfully performed by Ohmori et al. [Ohmori 1998b, 2002, 2004].

#### Isotope distribution

Isotopic distribution of Pd on the surface of the eight kinds of electrodes after the supra-electrolysis is shown in the figure [Ohmori 2016 (Fig.4)]. Without exception the isotopic abundance of the palladium electrodes deviates markedly from its natural one for all of the electrodes. In this, there are some common characteristics in the following: (i) Content of <sup>108</sup>Pd exceeds significantly its natural isotopic abundance for all of the electrodes: (ii) Content of <sup>110</sup>Pd exceeds its natural isotopic abundance in most cases,

(iii) In contrast, content of other lighter palladium isotopes are mostly below their natural isotopic abundance. Consequently, it appears that the content of heavier palladium isotopes tends to increase, whereas, the content of lighter ones tends to decrease.

### Foreign elements

Foreign elements with atomic numbers 2-4 larger, Cd and Sn, were detected after the supra-electrolysis of Pd electrode [Ohmori 2016 (Fig.7)]. The isotopic distribution of Cd is very different from its natural isotopic abundance. In this case,  $^{114}\text{Cd}$  (main isotopic component in natural Cd) was not contained in Cd detected after the electrolysis [Ohmori 2016(Fig.12)]. Isotopic distribution of Sn could not be analyzed because of overlapping of its SIMS signals with those of other materials)

Foreign elements with larger atomic numbers other than Cd and Sn, Pt and Au, were also detected. These elements have different isotopic distributions from their natural ones [Ohmori 2016 (Fig.9)]. In this electrolysis system, Pt net was used as a counter electrode. So the Pt was considered to be produced as a result of the electrodeposition of Pt dissolved from the counter electrode. The production of Au may result from the Pt like the production of Cd or Sn from Pd.

### 2.3 Normal Electrolysis with Au Cathode-Light Water System;

$\text{Au}/\text{H}_2\text{O} + \text{Na}_2\text{SO}_4 + \text{Na}_2\text{CO}_3 + \text{K}_2\text{CO}_3/\text{Pt}$

#### 2.3 (a) Experiment

The gold electrodes used were of Au sheets (1.0, 2.5 and 5.0  $\text{cm}^2$  apparent surface area). Electrolysis was carried out in 0.5M  $\text{Na}_2\text{CO}_3$ ,  $\text{Na}_2\text{SO}_4$ , and  $\text{K}_2\text{CO}_3$  solutions at current densities ranging from 0.1 to 0.5  $\text{A}/\text{cm}^2$ .

#### 2.3 (b) Precipitates

In the normal electrolysis (0.1  $\text{A}/\text{cm}^2$ ) no electrolysis deposits were observed. However, fine black porous precipitates began to appear at the bottom of the electrolytic cell when electrolyzed at current densities of  $> 0.2 \text{ A}/\text{cm}^2$ . In most cases the precipitates began to appear within 2-3 days after starting the electrolysis, and then gradually increased. The amount of the precipitates was in the range from 0.1 to 1 mg, and seemed to be different, depending on the slight difference in the manner of the surface pretreatment of the electrode. The scanning microscope (SEM) image of the precipitate is shown in [Ohmori 1997b (Fig.14)]. To all appearance, the precipitates look like fine black powder, but, in fact, they have a number of very fine porosities ranging from a few nm to  $\mu\text{m}$  order as shown in (b, c). —

書式変更: 蛍光ペン (なし)

The EPMA images are shown in [Ohmori 1997b (Fig.21)]. As seen from this figure the main component of the precipitates is gold. However other kinds of elements, such as Pt, Hg, Os, Hf, Fe and Si, are also included. Therefore, we can consider that these precipitates are those erupted from the volcano-like structure formed on the gold electrode as will be mentioned below.

### **2.3 (c) Surface topography of the electrode**

There have been observed many examples of topographical changes of cathode surfaces in experiments with normal and in supra-critical electrolysis [Silver 1993, Kozima 1998 (Appendix C7)]. The surface topography of electrodes observed in the experiments performed by Ohmori et al. [Ohmori 2016 (Secs, 3-2, 3-3, 4-2)] is discussed briefly in Sec. 4.3.2.

### **2.3 (d) Isotopic distribution of product elements**

The isotopic distribution of the major product elements reveals significant deviation from their natural isotopic abundance. The details will be described below.

#### **2.3 (d-1) Elements on/in the electrodes at low current densities**

Under the normal electrolysis at current densities  $> 0.2\text{A}/\text{cm}^2$ , no detectable precipitates appeared throughout the electrolysis. In this case iron atoms were detected exclusively at the part of the electrode close to the surface of the electrode. Figure 9 and 10 [Ohmori 1997b (Figs. 9 and 10)] show the AES spectra of the gold electrode after the electrolysis after 7 days of the electrolysis in  $\text{Na}_2\text{SO}_4$  and  $\text{K}_2\text{CO}_3$  at a current density of  $0.1\text{A}/\text{cm}^2$ . On the spectra of the uppermost layer iron and oxygen signals are observed other than gold signals. On carrying out  $\text{A}^+$  ion bombardment, the iron and oxygen signals decline, and disappear after several minutes. The distribution profile of iron atoms calculated from the results in Fig.9 is shown in Fig.12 [Ohmori 1997b (Fig. 12)].

#### **2.3 (d-2) Elements on/in the electrodes at high current densities**

A considerable amount of Hg is observed on and in the electrode after the normal electrolysis at higher current densities  $\sim 0.5\text{ A}/\text{cm}^2$ . Figure 17 [Ohmori 1997b (Fig.17)] shows EPMA mapping images of Au, Hg, Fe and Si on the gold electrode after the electrolysis in  $\text{Na}_2\text{CO}_3$  at a current density of  $0.5\text{ A}/\text{cm}^2$ . Judging from this figure the amount of mercury on the electrode surface is comparable with gold of the electrode material.

The isotopic abundance of the mercury is also different from its natural isotopic

abundance [Ohmori 1997b (Fig. 28)]. The content of lighter mercury isotopes,  $^{198}\text{Hg}$ ,  $^{200}\text{Hg}$  increase, while, the content of heavier ones,  $^{201}\text{Hg}$ ,  $^{202}\text{Hg}$ , decrease. Especially the maximum component,  $^{202}\text{Hg}$ , in the natural world decreases down to several percent.

### **2.3 (d-3) Elements on and in the precipitate produced in the electrolysis at high current densities**

The elements with anomalous isotopic distribution were also detected in the precipitant. As a typical example, we show the isotopic distribution of mercury against the scan number of SIMS [Ohmori 1997b (Fig.34)]. The content of  $^{200}\text{Hg}$  is much larger than its natural isotopic abundance also in this case although the isotopic distribution of mercury of the precipitant shows rather complicated as compared with that of Au electrode itself [Ohmori 1997b (Fig. 28)]. Perhaps such an abnormality is attributed to the structural feature of the precipitant. [Ohmori 1996a, 1996b, 1996c, 1997a, 1997b, 1998a]

### **2.4 Summary of the experimental data sets on the normal, critical and supra-critical electrolysis with 5d transition-metal cathodes**

There are more interesting features of the CFP than the nuclear transmutations analyzed in this paper. We explain some of them in addition to the summary of the nuclear transmutations explained above.

#### **2.4.1 Nuclear Transmutations in the 5d transition-metal cathodes**

It was necessary to perform electrolysis in critical and supra-critical conditions when the electrodes were 5d transition metals. Or it was necessary to use very long times of electrolysis. These conditions are discussed in Section 4.

#### **2.4.2 Surface topography**

There have been observed many evidences of nuclear reactions at surface regions of electrodes of CF materials. One of the most impressive evidence of nuclear reactions producing huge amount of excess energy has been the topography change of cathode surface showing such high temperatures above the melting points  $T_m$  of electrode metals as Ni ( $T_m = 1455\text{ }^\circ\text{C}$ ) and Pd ( $T_m = 1554.9\text{ }^\circ\text{C}$ ) in 3d and 4d transition metals (e.g. [Kozima 2006 (Fig. 2.3) and Appendix C7]).

Also, there have been observed topography changes of the cathode surface of 5d transition metals in the experiments where were observed nuclear transmutations; the melting points of these 5d transition metals are very high, i.e.  $T_m = 3387\text{ }^\circ\text{C}$  (W),  $T_m =$

3180 °C (Re),  $T_m = 1772$  °C (Pt) and  $T_m = 1064$  °C (Au). Some examples of them are briefly discussed below.

#### Gold cathode

The surface of the electrode after the electrolysis at a current density  $> 0.2$  A/cm<sup>2</sup> exhibits very anomalous structure. Figure 2.1 [Ohmori 1997b (Fig.40)] shows typical SEM images of the electrode surface before and after the electrolysis for 30 days at a current density of 0.5A/cm<sup>2</sup>.

Here (a) shows the electrode surface before the electrolysis. To our surprise a number of craters with various sizes are developed (Figures d and e). Each crater has a deep hole reminding us of a volcano. The size of the largest one reaches ca. 20  $\mu$ m diameter and 30  $\mu$ m height (b, c). From the appearance of these craters one can imagine that some explosion took place during the electrolysis, and as a result of this, such excellent craters were completed (f). The outside wall of the craters consists of fine porous substance which reminds us of the structure of the precipitates mentioned above. The inside of the craters at least consists of three kinds of layers as judged from the inspection of the picture, That is, while at the bottom part the wall is made of relatively large irregularly formed crystallites of several  $\mu$ m order, at the intermediate part the wall is made of more fine crystallites of several 100 nm order (g). The magnified picture of this layer shows that these crystallites have a hexagonal shape assignable to Au (111) (h). At the outside the wall consists of very fine crystallite of less than 30 nm. These crystallites also look hexagonal, although the outline is not necessarily clear. Hence these crystallites may be regarded as to be produced by the reconstruction of gold electrode material owing to the intense heat evolved.

Similar features have been observed in W and Re cathodes as briefly explained below.

#### Tungsten cathode

Surface topography of W electrode after the plasma electrolysis shows a crater-like structure [Ohmori 2016 (Fig.25)]. The EDX spectra were observed at two different spots on the crater-like structure; one is a spot A at the center part, and the other is a spot B near the edge. On the spectrum from spot A, strong signals of Fe and Cr and moderate signal of Ni are observed, from which the content of Fe, Cr and Ni are calculated as 67.4, 16.9 and 7.9 at.%, respectively. This suggests that the nuclear reaction takes place predominantly at the center of the crater.

### Rhenium cathode

Surface topography of Re electrode after the plasma electrolysis was investigated [Ohmori 2016 (Fig.20)]. A number of rhombus pits of various sizes are aligned with regularity. In addition, fine sharp grooves run straightly in all directions thrusting through the centers and corners of individual pits. The dimension of these pits is mostly in the range from 10 to 20 nm, respectively. On the surface of the electrode K, Zn, Fe and Cu were observed. [Ohmori 2000]

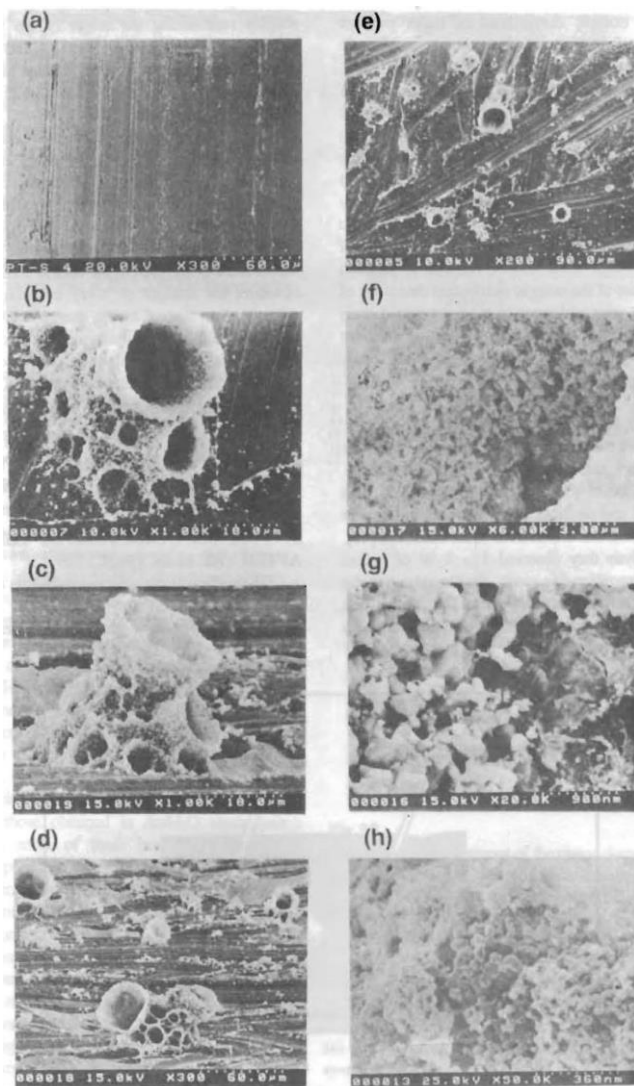


Fig. 2.1 Typical SEM images of the Au electrode surface before (a) and after (b) – (h) the electrolysis in Na<sub>2</sub>CO<sub>3</sub> solution of light water for 30 days at a current density of 0.5 A/cm<sup>2</sup> [Ohmori 1997b (Fig. 40)].

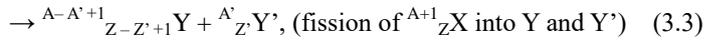
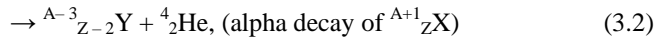
### 3. Trapped Neutron Catalyzed Fusion (TNCF) Model for the Cold Fusion Phenomenon (CFP)

The effectiveness of the TNCF model have already been shown by analyses of the CFP, especially the nuclear transmutations in such protium and deuterium systems as NiH and PdD using the idea of the neutron drop  ${}^A_Z\Delta$  [Kozima 2006 (Sec. 2.4.2), 2014a (Sec. 4)]. In this section, we summarize the essence of the TNCF model which will be used in Section 4 to analyze the experimental data obtained in 5d transition metal hydrides and deuterides.

#### 3.1 Phenomenological Model with an Adjustable Parameter $n_n$ , the Density of the Trapped Neutrons in a CF Material

Based on the curious experimental data showing occurrence of nuclear reactions in CF materials, we have elaborated a phenomenological model, the trapped neutron catalyzed fusion (TNCF) model, assuming several premises; the most important one of them is the existence of the trapped neutrons with a density  $n_n$  adjustable to an experimental data [Kozima 1994].

The fundamental nuclear reaction of the TNCF model is a reaction between a trapped neutron ( $n$ ) and a foreign or a displaced nucleus X ( ${}^A_ZX$ ) to generate a new nuclide Y ( ${}^{A+1}_ZX$ ) followed by some processes to generate a new nuclide Y or nuclides Y and Y', or others;



where  $\bar{\nu}_e$  is the anti-particle of the electron neutrino  $\nu_e$ .

This type of the nuclear transmutation (NT) is called the nuclear transmutation of the 1<sup>st</sup> kind (NT of type I) in this paper.

The TNCF model has been applied to a few data sets where were observed several observables (e.g. a and b) simultaneously; the quantitative relations between the values of the observables a and b have been explained by the model in a factor of 3 as expressed as follows;

$$(N_a/N_b)_{th} \cong m (N_a/N_b)_{ex}, \text{ (} m = 3 - 5). \quad (3.4)$$

where  $N_a$  and  $N_b$  are the values of observables a and b.

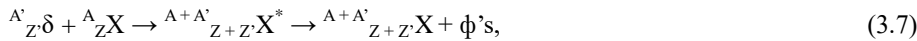
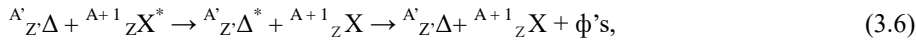
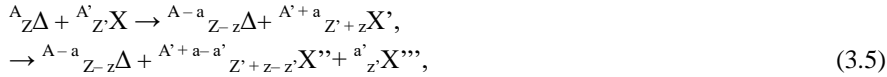
The resulting data of the analyses were tabulated in our books [Kozima 1998 (Tables 11.2 and 11.3), 2006 (Tables 2.2 and 2.3)]

This success of the model has shown that there is something true in the premises of the model reflecting reality in the cold fusion phenomenon (CFP).

### 3.1.1 Extension to the Neutron Drop Model

The success of the model described above encouraged extending the model to explain wonderful data sets of nuclear transmutations with large changes of proton Z and nucleon A numbers. Suggested by the work by Negele et al. [Negele 1973] on the neutron star matter, we proposed concepts of the CF-matter and the neutron drop  ${}^A_Z\Delta$  composed of Z protons and (A – Z) neutrons in the CF material [Kozima 1998 (Sec. 12.8), 2006 (Sec. 3.7), 2008b]. The CF-matter [Kozima 2006] is a concept to express a state composed of high density neutrons in the CF material similar to the neutron star matter in the case of the neutron star [Negele 1973].

When there are neutron drops in CF-matter formed around surface/boundary regions by the mechanism discussed above, we can use the neutron drop  ${}^A_Z\Delta$  and a small neutron-proton cluster  ${}^A_Z\delta$  in the nuclear reactions as a simultaneous feeder of several nucleons to nuclides. The nuclear transmutations (NT's) induced by this mechanism is called the nuclear transmutation of the 2<sup>nd</sup> kind (NT of type II) in this paper, and include following reactions;



In the reactions (3.6) and (3.7), we have used a symbol  $\phi$ 's to express dissipation of the excess energies in the intermediate neutron drop  ${}^{A'}_{Z'}\Delta^*$  and nuclide  ${}^{A+A'}_{Z+Z'} X^*$  into surrounding CF-matter (and then to the phonons in the lattice of CF materials) instead of photons in the case of nuclear reactions in free space.

The last reaction (3.8) is the transmutation by transformation (NT<sub>T</sub>) as classified according to the characteristics of nuclear reactions after the absorption of a neutron or of a neutron drop in the former papers (e.g. [Kozima 2014a]). In this case, a neutron drop  ${}^A_Z\Delta$  in a CF-matter transforms into a nuclide  ${}^A_Z X$  when it suffered disturbance by a foreign nucleus or displaced nucleus at a surface region or in a volume of the superlattice where the CF-matter exists.

In these nuclear reactions, a neutron drop can participate in them resulting in the nuclear transmutations such as  ${}^A_{79}\text{Pd} \rightarrow {}^A_{82}\text{Pb}$  [Ohmori 1998a].

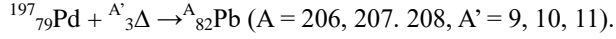


Table 3.1 Nuclear transmutations in the cold fusion phenomenon (CFP) arranged according to the nuclear processes from the initial to the final stages; a, initial, b, intermediate, and c, final stages. Nuclear transmutations by decay ( $\text{NT}_D$ ), by absorption ( $\text{NT}_A$ ), by transformation ( $\text{NT}_T$ ), and fission ( $\text{NT}_F$ ), which have been used in the former books and papers (e.g. [Kozima 1998, 2006, 2014a]) are used to describe the final reactions to assist understanding of the complex nature of the NTs in the CFP.  $\bar{\nu}_e$  is the anti-particle of the electron neutrino.

Initial reactants in the stage a of NT and (its classification)	Intermediate nuclide in the stage b	Final reaction products in the stage c (common to NT I and NT II are omitted)	Classification by the final reaction in the stage c
$n + {}^A_Z\text{X}$ (NT I)	${}^{A+1}_Z\text{X}^*$	${}^{A+1}_Z\text{X}' + e^- + \bar{\nu}_e$ ${}^{A-3}_{Z-2}\text{X}' + {}^4_2\text{He}$ ${}^{A+1}_Z\text{X} + \phi$ 's	$\text{NT}_D(\beta)$ $\text{NT}_D(\alpha)$ $\text{NT}_A(\phi)$
${}^{A'}_{Z'}\Delta + {}^A_Z\text{X}$ (NT II)	${}^{A+A'}_{Z+Z'}\text{X}'^*$	${}^{A+A'-a'}_{Z+Z'-z'}\text{X}'' +$ ${}^{a'}_{z'}\text{X}''' + \phi$ 's	$\text{NT}_F$
${}^{A'}_{Z'}\Delta$ (NT II)	${}^A_Z\text{X}^*$	${}^A_Z\text{X} + \phi$ 's	$\text{NT}_T$

The scheme of the nuclear transmutations grasped by the TNCF model is tabulated in Table 3.1.

We are able to clarify the nature of the CF-matter in relation to the NTs of the first kind (NT I) and the second kind (NT II). It is shown that the physical meaning of the two types of the CF-matter, type-I and type-II. The former is formed in CF materials when electrolysis is done with relatively low current density, and responsible for NT I, while the latter is formed there when electrolysis is performed with relatively large current densities including critical electrolysis and supra-critical electrolysis (glow and arc discharges), and results in NT II. The type-I CF-matter seems to correspond to the neutron star matter at lower density while the type-II CF-matter to the neutron star matter at higher density as shown by simulation by Suess and Urey [Suess 1956].

### 3.2 Foundation of the TNCF Model

It has been a common sense in physics that the environment in a crystal around an interstitial proton/deuteron does not have strong influence on the two-body interaction between a lattice nucleus and an interstitial proton/deuteron [Kozima 1998 (Sec 12.2d), 2006 (Sec. 3.4.3)]. However, the investigation of the bases of the TNCF model, a part of which was given in the former book [Kozima 1998 (Secs. 12.4 – 12.8)], has given us an idea of the super-nuclear interactions between lattice nuclei mediated by interstitial protons/deuterons which results in formation of neutron energy bands presupposed before [Kozima 1998 (Sec. 12.4)]. The super-nuclear interaction has a similarity in the superexchange interaction between Mn ions mediated by oxygen ions in MnO anti-ferromagnetism (e.g. [Suzuki 2009 (Introduction), Timm 2009 (Sec. 4.3)]). Thus, it was shown that the two neutrons at lattice points far out of the range of nuclear force of about one fermi ( $= 10^{-15}$  m) can interact each other by the mediation of wavefunctions of a proton (or a deuteron) at interstitial sites extended to the lattice points where are the neutrons.

Furthermore, the exotic nuclei with large excess of neutron numbers over those of stable nuclei have recently investigated extensively. Existence of these exotic nuclei with extended distribution of excess neutrons has encouraged the investigation of the super-nuclear interaction [Kozima 2006 (Sec. 3.7), 2008b, 2009].

### **3.2.1 The Super-nuclear Interaction between Lattice Nuclei mediated by Interstitial Protons/Deuterons**

There is another factor which encouraged the calculation of the super-nuclear interaction; the extension of proton/deuteron wavefunctions in an interstitial sites in fcc transition metals. It is well known that wavefunctions of proton and deuteron in Pd, one of the best investigated transition-metal hydrides, are not localized at the interstitial sites but extended to overlap with neighbouring lattice points.

On the other hand, neutrons in an outermost shell of a lattice nucleus have rather extended wavefunctions, especially when the nucleus is in an exotic state; a state with a large excess number ( $A - Z$ ) of neutrons over the number  $Z$  of protons;  $(A - Z) \gg Z$ . Therefore, the extended distribution of the neutrons in an outermost shell of a lattice nucleus (possibly an exotic nucleus) and the non-localized wavefunctions of interstitial protons/deuterons are favorable for the super-nuclear interaction to realize the neutron energy bands [Kozima 2006 (Sec. 3.7), 2008b, 2009].

### **3.2.2 Formation of the Neutron Energy Bands and CF-Matter**

Once the neutron energy bands are formed by lattice neutrons (neutrons in lattice

nuclei) with the super-nuclear interaction, the neutrons in the neutron valence band accumulate at boundary/surface regions of the CF material to form a CF-matter with a density around  $10^8 - 10^{12} \text{ cm}^{-3}$  as determined by the analyses of experimental data sets [Kozima 1998 (Tables 11. 2 and 11.3), 2006 (Tables 2.2 and 2.3).

It should be emphasized again here that the neutrons in a neutron energy band do not interact with lattice nuclei such as Pd and Ni in PdD or NiH as described by the Bloch Theorem [Seitz 1940, Kittel 1976]. They interact with foreign nuclei at crystal surfaces or disordered nuclei from lattice points of the CF-material. This is the cause of the localized appearance of the fusion products in the CFP.

This simple fact has been forgotten in researchers in the field of CFP, even if it has been clearly written down in textbooks for instance as follows;

“These solutions are composed of traveling waves, and they can be assembled into wave packets to represent electrons that propagate freely through the potential field of the ion cores.” [Kittel 1976 (p. 190)]

### **3.3 CFP in CF Materials by the CF-Matter Formation**

Thus, from our point of view, it is necessary to have the CF-matter by any means to realize the CFP in a CF material. In order of preparation of the CF material, we can enumerate the necessary conditions for the realization of this state as follows.

#### **Necessary Conditions for and Characteristics of the CFP in CF materials:**

(1) Absorption of protium/deuterium into the material (at least in the surface regions thicker than at least about  $200 \text{ \AA} = 20 \text{ nm}$ ) with a density as high as that of the host element [Kozima 2000 (Sec. 4)]. It is said that the necessary average density of the hydrogen isotopes should be larger than a minimum value, given for instance by the composition ratio  $D/Pd > 0.7$  in the case of  $PdD_x$  [McKubre 1993].

(2) Formation of the superlattice composed of a sublattice of the host nuclei at the lattice points and another sublattice of protons/deuterons at the interstitial sites in localized regions of the material. The self-organization, a cooperative process, might be relevant to this superlattice formation [Kozima 2013, 2016b (Sec. 3.8)]. This condition relates closely with a characteristic of the complexity, and is one of the most effective causes for the qualitative reproducibility, i.e. the lack of the quantitative reproducibility. We can expect at best only a qualitative reproducibility in the CFP which is in accordance with the notorious irreproducibility of events in the CFP.

(3) Existence of lattice nuclei with neutrons at evaporation levels (where the exotic nuclei are favorable) [Kozima 2016c]. The neutrons in the outermost shell of a lattice

nucleus may be responsible for the super-nuclear interaction explained below.

(4) Existence of non-localized proton/deuteron wavefunctions in the material. It is probable that the higher the diffusivity of protons/deuterons, the larger the extension of their wavefunctions, from experimental data in solid state physics [Kozima 2009]. This is the reason that the CFP is frequently observed in hydrogen occluding transition-metals at near room temperature.

(5) Realization of the super-nuclear interaction between lattice nuclei (mediated by interstitial protons/deuterons) [Kozima 2006 (Sec. 3.7.2), 2016c (Sec. 5.2.3)]. Overlapping of a proton/deuteron wavefunction and a neutron wavefunction results in the attractive interaction of the proton/deuteron and the neutron in the first order, and then in the super-nuclear interaction between two neutrons in different lattice nuclei in the second order approximation.

(6) Formation of the neutron energy bands by the coupled neutrons with the super-nuclear interaction [Kozima 2006 (Sec. 3.7), 2016c], Mediation of the super-nuclear interaction is realized by the interstitial hydrogen isotopes in transition-metal hydrides/deuterides or by the hydrogen atoms of organic molecules in the polyethylenes and biological cultures.

(7) Supply of neutrons into one (valence band) of the formed neutron energy bands [Kozima 1998 (Sec. 8.3), Kozima 2006]. Neutrons may be supplied by excitation from lower energy levels of lattice nuclei or by neutrons from outside absorbed by the CF material.

(8) Accumulation of neutrons at boundary/surface region of the CF material to form the CF-matter [Kozima 2006 (Sec. 3.7.2.3), 2011, 2016b (Sec. 3.5)]. It is recognized that the CF-matter is classified into two kinds; (1) type-I CF-matter where occur nuclear transmutations of the 1<sup>st</sup> kind (participation of a single neutron) only and (2) type-II CF-matter where occur nuclear transmutations of the 2<sup>nd</sup> kind (in addition to that of the 1<sup>st</sup> kind) with participation of a neutron drop  ${}^A_Z\Delta$  (cf. Sec. 4).

(9) Strong interaction between particles in the CF-matter is responsible for the dissipation of excess energies liberated by nuclear reactions of the 1<sup>st</sup> and 2<sup>nd</sup> kinds the results of which are observed as nuclear transmutations. This could be one of the reasons why we do not observe radiations after nuclear reactions that are unavoidable in free space.

(10) Interaction of neutrons in the neutron energy bands with disordered nuclei and with foreign nuclei [Kozima 2016c (Sec. 5.2)]. It needs hardly be said that the neutrons in the neutron energy bands do not interact with lattice nuclei at their regular array as its nature but interact with nuclei in such disordered sites as displaced positions in the

lattice and at boundary regions. This is the cause of localization of nuclear reactions at surface/boundary regions which have observed frequently in experiments.

Nuclear transmutations observed hitherto in CF materials have been explained at least qualitatively and quantitatively sometimes by the TNCF model [Kozima 1998, 2006, 2009, 2014a (Sec. 4), 2016c].

A word should be mentioned on the relation of the CF-matter proposed in our model and the neutron star matter investigated in nuclear physics. The neutron star matter has been taken up in the investigation of the neutron star (e.g. [Suess 1956]) and treated in a uniform space without boundary. On the other hand, the CF-matter is formed by neutrons in neutron energy bands made of neutron eigenfunctions in lattice nuclei in a superlattice with irregularities and boundaries by which the arrangement of the superlattice is disturbed. These disturbances on the CF-matter surly cause perturbation on the behavior of neutrons in the CF-matter, and become causes of interactions between the neutron drops and foreign nuclides resulting in the nuclear reactions described in Eqs. (3.4) – (3.8). This scenario is told by phantasy on the basis of the successful explanation of the CFP by the TNCF model, and should be explained quantitatively by mathematics which seems to acquire tremendous works on the computer. We have to wait anyone dares to do this work.

#### **4. Analysis of the Data of the Nuclear Transmutations (NTs) by the TNCF Model**

The experimental results on the nuclear transmutation in critical and supra-critical electrolysis are analyzed and interpreted using the TNCF model in consistency with other data in the cold fusion phenomenon in 3d and 4d transition-metal hydrides and deuterides charged by the normal electrolysis and gas contact method.

##### **4.1 Necessity of critical and supra-critical electrolysis for such CF materials as Graphite and 5d transition-metals**

As is well known in the history of CF research in these more than 25 years, such 3d and 4d transition metals as Ti, Ni and Pd used in the CF experiments at the normal electrolysis condition are known as hydrogen occluding metals where hydrogen isotopes are absorbed into the metal, and form alloys with the host element (occluded). Generally speaking, in these alloys, protons/deuterons have high diffusivity, and their wavefunctions are not localized at an interstitial site but extend out to cover the lattice sites where are the nuclei of the host element.

On the other hand, as shown in Appendix A, the CF materials such as graphite and 5d transition-metals do not occlude hydrogen isotopes at near room temperature, and have not been much investigated as the materials in relation to the occlusion of hydrogen isotopes. However, at higher temperatures above several hundred °C, physical properties of these materials become similar to the 3d and 4d transition-metal hydrides/deuterides at near room temperature, as shown partly in Appendix A.

Therefore, the theoretical investigation based on the TNCF model explained in Section 3 predicts that the graphite and 5d transition metals will be CF materials at higher temperatures where they have ability to occlude enough amount of hydrogen isotopes.

Here is an interesting prediction we are able to deduce from the necessary conditions given in Subsection 3.3. The necessary conditions for realization of the CFP in CF materials tell us that it is necessary to form hydrides with a large ratio (e.g. H/W in  $WH_x$  compound with  $x \sim 1$ ) of proton/deuteron to host metal. The Necessary Condition (2) demands a lower limit for the density of protium in the CF material to form a superlattice by a cooperative process. Then, there should be a threshold value of the input power  $\varepsilon_{th}$  (a product  $i_{th} \times V_{th}$  of the current density  $i_{th}$  and voltage  $V_{th}$ ) of electrolysis (e.g. in Au/H<sub>2</sub>O/Pt system) and the threshold duration  $\tau_{th}$  of electrolysis for realization of the CFP.

About the effect of the input power  $\varepsilon$  and the duration of electrolysis  $\tau$  on the CF-matter formation (Necessary Condition (8)), we will be able to take up the product of the two quantities,  $P \equiv (\varepsilon \times \tau)$ , in a rough estimation. To feed enough amount of protium/deuterium to CF materials which have positive heats of solution (W, Pt and Au as shown in Fig. A1), it is necessary to have a larger  $\varepsilon \times \tau$  value larger than a threshold value  $P_{th} = \varepsilon_{th} \times \tau_{th}$ . Then, the condition (8) is written down as an inequality  $\varepsilon \times \tau > P_{th}$ . The area of  $\varepsilon$  and  $\tau$  satisfying this condition is shown schematically in Fig. 4.1 above the line  $P_{th} = \varepsilon \times \tau$  (with  $\varepsilon \equiv x$ ,  $\tau \equiv y$ , and  $P_{th} = 1$ ).

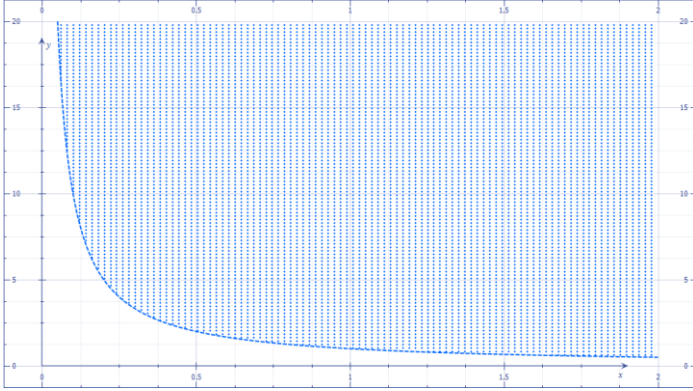


Fig. 4.1 The region  $\epsilon \times \tau > P$  is shown schematically in this non-dimensional figure as the area above the dotted curve  $\epsilon \times \tau = P_{th} = 1$  ( $\epsilon = x$ ,  $\tau = y$ , and  $P_{th} = 1$ ). In this region, it is possible to satisfy the necessary condition (8) and to realize the CFP according to the TNCF model.

There are no systematic investigations of the behavior of the CF materials about this relation depicted in Fig. 4.1 yet. However, we are able to speculate some quantitative relations on the limiting behavior of the input power  $\epsilon_{th}$  and the threshold duration  $\tau_{th}$  of electrolysis in Au/H<sub>2</sub>O/Pt systems. The relations of the input cell voltage and the elapsed time are shown in Fig. 4.2 for an experiment with the electrolysis current density of 0.2 A/cm<sup>2</sup>. From these data shown in Fig. 4.2, we may tentatively take  $\epsilon_{th} \sim 0.2 \times 5 \text{ AV/cm}^2$  and  $\tau_{th} \sim 3600 \text{ s}$ , and therefore  $P_{th} \sim 3.6 \times 10^3 \text{ AVs/cm}^2$ .

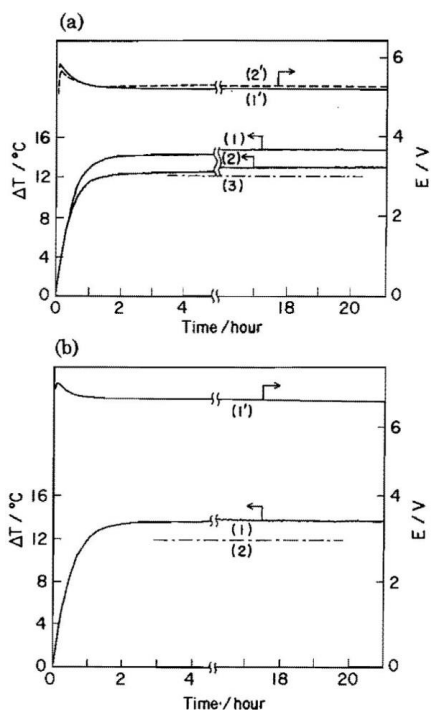


Fig. 4.2 The temporal dependences of the solution temperature (1) – (3) and the input potential (1') – (2') after starting electrolysis on gold electrodes: In Fig. 4.2 (a), (1) and (1') for  $\text{H}_2\text{O} + \text{Na}_2\text{SO}_4$ , (2) and (2') for  $\text{H}_2\text{O} + \text{K}_2\text{CO}_3$ , and the temperature level (3) when  $P_{\text{ex}} = 0$ ; In Fig. 4.2 (b), (1) and (1') for  $\text{D}_2\text{O} + \text{K}_2\text{CO}_3$ , while (2) the temperature level when  $P_{\text{ex}} = 0$  (after [Ohmori 1997b (Fig. 2)]).

Qualitatively, this prediction is consistent with experimental facts; (1) In the case of graphite,  $P$  should be very large as given by the arc discharge, (2) in the case of Au, it is necessary to have large values of  $\tau$  (by long term electrolysis) to make the  $P$  large, (3) in the case of W and Pt, it is necessary to have critical and supra-critical electrolysis to have a large value of  $\varepsilon$  to make the  $P$  large. In the case of Pd/ $\text{H}_2\text{O}$ /Pt system, we need a larger  $\varepsilon$  by a longer electrolysis time or by a larger current density than in the case of Pd/ $\text{D}_2\text{O}$ /Pt system.

This prediction will be best illustrated by the extensive experiment with Au/ $\text{H}_2\text{O}$ /Pt system performed by Ohmori et al. (cf. Sec. 2.3 and [Ohmori 1997b]).

#### 4.2 Analysis of the experimental data sets on the nuclear transmutation in normal, critical and supra-critical electrolysis with graphite, W, Re, Au and Pd cathodes.

The nuclear transmutation (NT) is the most remarkable and astonishing facts we

encountered in the experimental results obtained in the CFP, and we have given a unified explanation for the whole data sets on them using the TNCf model [Kozima 1998 (Sections 11.11 and 11.12), 2006 (Sec. 2.5), 2011b, 2014a]. Especially, the abundant production of iron isotopes with similar isotopic abundances to the natural ones suggested the nature of the CF-matter in this case is similar to the environment where the elements were composed in nature as pointed out before [Kozima 2011b].

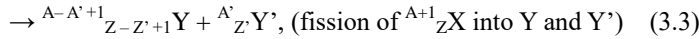
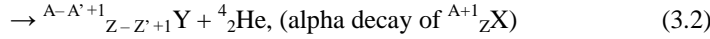
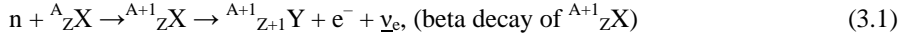
Thus, the explanation of extraordinary data sets obtained in the papers taken up here depends largely on “the stability law” concluded from experimental data as formulated by us [Kozima 2011b], and is necessarily qualitative.

#### 4.2.1 Nuclear Transmutations (NT) in the Cold Fusion Phenomenon in General

Explanation of the experimental data sets presented in Sec. 2 is given in this Section using the TNCf model (Sec. 3.1) taking into consideration the facts of occluded H/D in metals given in Sec. 3.2. Especially the data sets obtained in Pd and Au cathodes are discussed in the Section 4.2.2.1 and 4.2.2.2, respectively, for their interesting features among others.

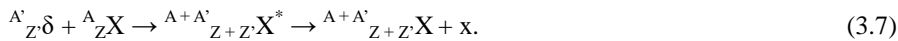
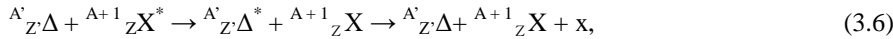
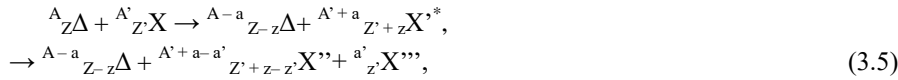
Fundamental nuclear reactions used for the explanation of experimental data are following ones (1) NT of the 1<sup>st</sup> kind (NT I) where participates a single neutron assumed in our original TNCf model and (2) NT of the 2<sup>nd</sup> kind (NT II) where participates a neutron drop assumed in our extended model (cf. Section 3.1);

(1) NT of the 1<sup>st</sup> kind (NT I),



and

(2) NT of the 2<sup>nd</sup> kind (NT II),



Where  $\bar{\nu}_e$  is the anti-electron neutrino.

Then, we can explain the data of nuclear transmutations observed in the 5d transition-metal cathodes using these reactions (3.1) – (3.3) and (3.5) – (3.8).

We give only several examples of explanation in this Section. At first, we give a part of the abundance of elements in universe is tabulated in Table 4.1 [Suess 1956] for

convenience of later discussion. In this table,  $\log_{10}H$  means the abundance of elements in universe, and Fe is at a marked peak of the  $\log_{10}H$  vs. Z diagram (cf. [Kozima 2006 (Fig. 2.11)] for the whole diagram).

Table 4.1 Peaks of  $\log_{10}H$  of elements in the universe [Suess 1956].

<b>Z</b>	13	14	20	24	25	26	28	29	30
<b>Element</b>	Al	Si	Ca	Cr	Mn	Fe	Ni	Cu	Zn

**(a) The nuclear transmutation in graphite/H<sub>2</sub>O system at arc discharge**

The experimental data sets obtained in graphite-H<sub>2</sub>O system have been analyzed using the TNCF model before [Kozima 2012]. Here, we discuss only a data of isotopic abundance of iron isotopes generated in the graphite-H<sub>2</sub>O system. The isotopic ratios of iron generated in the experiments were the same as that of the natural ones. This correspondence of the products of CF reactions and the primordial production of elements in nature has been interpreted to show an interesting fact of “the stability law” deduced from an overall comparison of CF data with the abundance of elements in universe [Kozima 2011b].

**(b) Data from experiments with W/H<sub>2</sub>O+Na<sub>2</sub>SO<sub>4</sub>/Pt system [Ohmori 2000b]**

Here, we take up only the production of  $^{A}_{26}\text{Fe}$  and  $^{A}_{75}\text{Re}$  from the data obtained and tabulated in Table 2.1. The A and Z of nuclides relevant to this system should be noticed at first;  $^{A}_{74}\text{W}$  (A = 180 – 186),  $^{A}_{11}\text{Na}$  (A = 23),  $^{A}_{78}\text{Pt}$  (A = 190 – 198).

**(b1)  $^{56}\text{Fe}$  and  $^{57}\text{Fe}$  with similar isotopic abundances to the natural ones.**

This characteristic of isotopic abundances of the product Fe presented in Sec. 2.1.3 is noticed several times before (e.g. (a) above), and suggested the nature of the CF-matter resembling to the environment when elements were formed in nature. The CF-matter comprises neutron drops  $^{A}_{Z}\Delta$  with extensive values of A and Z. It is conceivable that the nuclear reaction occurs where occurs a transformation reaction from a neutron drop to a nucleus (3.8) with a large probability for abundant A and Z according to the stability effect;

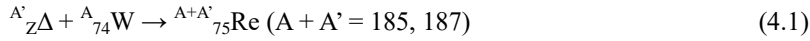


**(b2)  $^{185}_{75}\text{Re}$  and  $^{187}_{75}\text{Re}$  with different isotopic abundances from the natural ones.**

Let us check the natural abundances of these product isotopes first; their natural abundances are 37.07 and 62.93 (with a ratio **0.59**) while the detected abundances are **48.4 and 51.6**, respectively. The ratio of the abundances of the products is  $48.4/51.6 =$

**0.94**, higher than the natural case by a factor of 1.6.

The simplest reactions producing  ${}^A_{75}\text{Re}$  from the cathode elements  ${}^A_{74}\text{W}$  is the following;



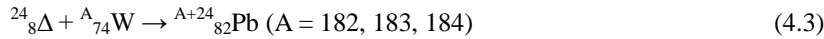
Let us take tentatively  $A = 184$  and  $186$  to meet the experimental results  $A + A' = 185$  and  $187$ . Then, the neutron drop participating in the reaction (3.8) is  ${}^1_0\Delta = n$ , and the products reflect the abundances of  ${}^A_{74}\text{W}$  ( $A = 184$  and  $186$ ) which are **30.64** and **28.41**. The ratio of these abundances is **1.08**. This value is compared to the observed value **0.94** closer than the natural value 0.59. This result suggests favorable ability of the TNC model, if the products  ${}^A_{75}\text{Re}$  directly reflect the originals  ${}^A_{74}\text{W}$ . This point is discussed further in Section 4.5.

It should be noticed that there are possibilities generating  ${}^A_{75}\text{Re}$  directly by transformation of the neutron drop in addition to these reactions (4.1);



### (b3) ${}^A_{82}\text{Pb}$ with different isotopic abundances from the natural ones

There are three isotopes of lead  ${}^A_{82}\text{Pb}$  ( $A = 206, 207$  and  $208$ ) found in the surface layers of W cathode with abundances 38.5, 55.0 and 6.5 compared to the natural once 25, 22 and 52, respectively. A candidate of the reactions producing these lead isotopes from the tungsten isotopes are following;



It is interesting to notice a fact appeared here that a neutron drop with a proton number  $Z$  of a multiple of 2 and a nucleon number  $A$  of a multiple of 4. These kinds of neutron drops are frequently encountered in past in the analyses of experimental data of the nuclear transmutation (e.g. [Kozima 2014a (Sec. 5.2)]).

### (c) Data from experiments with $\text{Re}/\text{H}_2\text{O}+\text{K}_2\text{CO}_3/\text{Pt}$ system [Ohmori 2000a]

The experimental data obtained by Ohmori et al. [Ohmori 2000a] show that there are detected new elements  ${}^A_{26}\text{Fe}$  and  ${}^A_{29}\text{Cu}$  or  ${}^A_{30}\text{Zn}$  in different electrodes. The  $A$  and  $Z$  of nuclides relevant to the original system should be noticed at first;  ${}^A_{75}\text{Re}$  ( $A = 185, 187$ ),  ${}^A_{19}\text{K}$  ( $A = 39, 40, 41$ ) and  ${}^A_{78}\text{Pt}$  ( $A = 190 - 198$ ).

The production of Fe is interpreted similarly to the case of (a) graphite and (b) W cathodes. The productions of Cu and Zn also may be explained by the stability law using the data shown in Table 4.1. The elements Fe, Cu and Zn are at peaks of the  $\log_{10}H$  vs.  $Z$  diagram. The accidental appearance of Fe and Cu or Zn in this experiment may reflect the unknown nature of the CF-matter formed at the surface region of Re

cathodes.

#### 4.2.2 Specific Explanation of the Data Sets obtained in Pd and Au Cathodes

The data sets obtained in the Pd and Au cathodes are given in this section due to their extensive and interesting features showing several characteristics of the CFP in electrolytic systems.

##### 4.2.2.1 Pd Cathode

The experimental results on the systems with Pd cathodes are introduced in Sec. 2.1.2. There are two types of experiments with the Pd cathode, one in the system Pd/D<sub>2</sub>O/Pt and another in Pd/H<sub>2</sub>O/Pt system.

###### (a) Pd/D<sub>2</sub>O+Li<sub>2</sub>CO<sub>3</sub>/Pt with current densities of 0.2 – 0.8 A/cm<sup>2</sup> [Mizuno 1998].

In this experiment, the current density was below the limit of the critical electrolysis, but reaches to the limit as the authors call the condition “Strong Electrolysis” in the title of the paper [Mizuno 1998]. This condition of the experiment seems reflected in the experimental results as explained below.

The abundant production of 3d transition-metals may be the result of the stability effect reflecting the log<sub>10</sub>H peaks shown in Table 4.1. This may show the excited or turbulent state of the CF-matter in the Pd surface layers in this experimental condition.

On the contrary to the case 4.2.1a graphite/H<sub>2</sub>O/graphite and 4.2.1b W/H<sub>2</sub>O/Pt systems where was observed generation of iron isotopes <sup>56</sup>Fe with the same isotopic abundances to the natural ones, the data of <sup>54</sup>Cr had shown difference from the natural abundances. This may be an indication of weaker turbulence of the CF-matter in this Pd/D<sub>2</sub>O+Li<sub>2</sub>CO<sub>3</sub>/Pt system than those in graphite/H<sub>2</sub>O/graphite and W/H<sub>2</sub>O/Pt systems considered in Sections 4.2.1a and 4.2.1b.

###### (b) Pd/H<sub>2</sub>O+Na<sub>2</sub>SO<sub>4</sub>/Pt with critical electrolysis at current density of 2 A/cm<sup>2</sup> [Ohmori 1997b, 2016]

The experimental data in this system include many facts related to the nuclear reactions occurring in the surface layers in Pd cathodes at the critical electrolysis. It is certain from discussions given in the above sections that the CF-matter in this case is rather turbulent than the CF-matter formed in cases of normal electrolysis considered in our papers and books before [Kozima 1998, 2006, 2014a]. We take up two data sets in this system leaving other results common to results in other papers analyzed in other subsections in this Section 4.2.

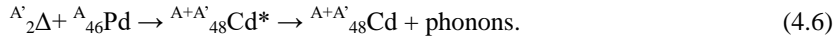
###### (b1) Isotopic abundances of Pd in surface layers

Experimental result shows that the content of heavier palladium isotopes tends to increase, whereas the content of lighter ones tends to decrease. This qualitative tendency of upwards shift of isotopic abundances of palladium  ${}^A_{46}\text{Pd}$  is a natural result of following reactions of a neutron and palladium nuclide, but is complicated by the reactions following the formation of intermediate nuclide  ${}^{A+1}_{46}\text{Pd}^*$ ;



### (b2) Isotopic abundances of ${}^A_{48}\text{Cd}$ generated in surface layers

The generation of cadmium from Pd is most simply explained by the reaction between a neutron drop and a palladium nuclide  ${}^A_{46}\text{Pd}$ ;



The intermediate nuclide  ${}^{A+A'}_{48}\text{Cd}^*$  is in the CF-matter surrounding it, and is succeeded by reactions expensing excess energy liberated at the second step to the lattice instead of a photon in the case of free space.

Experimental data of isotopic abundance of cadmium  ${}^A_{48}\text{Cd}$  is tabulated in Table 4.2 using the data given in [Ohmori 2016].

Table 4.2 Isotopic Abundances (%) of  ${}^A_{48}\text{Cd}$ . Natural abundance  $x_{0A}$  and the average value  $\underline{x}_A$  of two values obtained at two points on the sample surface in the experiment [Ohmori 2016 (Fig. 12)] are tabulated according to the atomic number A. The measured abundance  $\underline{x}_A$  (%) is read out from the original data given as a histogram [Ohmori (Fig. 12)].

A of Cd isotope ${}^A_{48}\text{Cd}$	110	111	112	113	114	116
Natural abundance $x_{0A}$ (%)	12.39	12.75	24.07	12.26	28.86	7.58
Measured abundance $\underline{x}_A$ (%)	0	<b>8</b>	<b>34</b>	<b>56</b>	0	0

Table 4.3 Natural abundances  $x_{0A}$  (%) and absorption cross sections for a thermal neutron (barns) of  ${}^A_{46}\text{Pd}$ .

A of Pd isotope ${}^A_{46}\text{Pd}$	102	104	105	106	108	110
Natural abundance $x_{0A}$ (%)	0.98	<b>11.0</b>	<b>22.3</b>	<b>27.3</b>	26.7	11.8
Absorption cross-section (barn)	3.36	0.52	20.2	0.30	8.50	0.22

To investigate further details of the reaction (4.6), we tabulate here the isotopic abundances  $x_0$  (%) and absorption cross sections  $\sigma$  of palladium  ${}^A_{46}\text{Pd}$  for a thermal neutron (barns) in Table 4.3.

The correspondence of the experimental result on Cd (Table 4.2) and the data of Pd in the cathode Pd (Table 4.3) suggests the simplest possible mechanism that the products

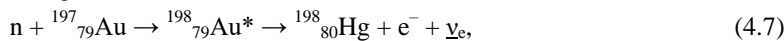
${}^A_{48}\text{Cd}$  ( $A = 11, 112, 113$ ) are the results of the absorption of  ${}^7_2\Delta$  ( $A' = 7$ ) in the reaction (4.6) by palladium isotopes  ${}^A_{46}\text{Pd}$  ( $A = 104, 105, 106$ ). Then, we can deduce an interesting conclusion on the interaction of a neutron drop and a nucleus; the dependence of the probability of the absorption of  ${}^7_2\Delta$  by  ${}^A_{46}\text{Pd}$  on  $A$  ( $A = 104, 105, 106$ ) is proportional to  $8/11.0 = 0.73$ ,  $34/22.3 = 1.53$ ,  $56/27.3 = 2.05$ , respectively. Their ratio is (1: 2.1: 2.8). It is clear that the absorption cross-sections of  ${}^7_2\Delta$  by  ${}^A_{46}\text{Pd}$  ( $A = 104, 105$  and  $106$ ) are independent of the corresponding absorption cross-sections (0.52, 20.2 and 0.30 b) of single thermal neutron tabulated in Table 4.3 with their ratio of (1: 38.8: 0.6).

The supposed participation of the neutron drop  ${}^7_2\Delta$  is a rare case we met hitherto. The most abundant cases of nuclear transmutations are explained by participation of neutron drops with even values of nucleon numbers  $A$  such as  ${}^4_2\Delta$  and  ${}^8_2\Delta$ . This may be another exceptional characteristic of a turbulent CF-matter formed in critical electrolysis.

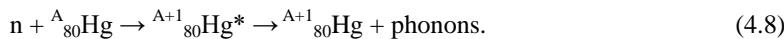
#### 4.2.2.2 Au Cathode

The experimental results introduced in Sec. 2.3 shows that the isotopic abundance of the mercury is different from its natural isotopic abundance [Ohmori 1997b (Fig. 28)]. The content of lighter mercury isotopes,  ${}^{198}_{80}\text{Hg}$ ,  ${}^{200}_{80}\text{Hg}$  increase, while, the content of heavier ones,  ${}^{201}_{80}\text{Hg}$ ,  ${}^{202}_{80}\text{Hg}$ , decrease. Especially the maximum component,  ${}^{202}_{80}\text{Hg}$ , in the natural world decreases down to several percent.

The most probable nuclear reactions generating mercury isotope  ${}^A_{80}\text{Hg}$  from the cathode element, gold with only one isotope  ${}^{197}_{79}\text{Au}$ , from our point of view is the following;



with a fairly large neutron absorption cross-section  $\sim 98.9$  barn (if it is applicable to this case). The product nuclide  ${}^{198}_{80}\text{Hg}$  in the CF material is in the CF-matter surrounding it, and is succeeded by reactions expensing excess energy liberated at the second step to the to the lattice instead of a photon in the case of free space.



Here, we cite several data of nuclear physics supposed to be relevant to further consideration.

Natural abundances of mercury is tabulated in Table 4.4 together with those obtained in the Au electrode after the experiment [Ohmori 1997b (Fig. 28)]. This table shows clearly that the detected mercury nuclei have their origin in the CFP but not in

contamination or other artifacts.

Table 4.4 Isotopic Abundances of  ${}^A_{80}\text{Hg}$ , Natural abundance and data obtained in the experiment [Ohmori 1997b (Fig. 28)]

Nucleon number $A$	196	198	199	200	201	202	204
Natural abundance $x_{0i}$ (%)	0.15	9.97	16.87	23.10	13.18	29.86	6.87
Experimental abundance $x_i$ (%)		<b>21</b>	15	<b>57</b>	6	5	5

The data of isotopic abundance of product mercury may be tentatively explained using the single neutron reactions (4.7) and (4.8) given above as follows. (It should be remembered that there are other possible reactions induced by neutron drops  ${}^A_Z\Delta$  with  $A > 1$  and  $Z \geq 0$ ). We may use the cross-sections  $\sigma_{\text{nHg}}^{(A)}$  of neutron absorption by a nucleus  ${}^A_{80}\text{Hg}$  given in Table 4.5 and that of  ${}^{197}_{79}\text{Au} \sim 98.9$  barn in these reactions. The first step is naturally the production of  ${}^{198}_{80}\text{Hg}$  by the reaction (4.7). The density  $x_0(t)$  of gold nucleus  ${}^{197}_{79}\text{Au}$  decreases according to the following equation as depicted in Fig. 4.3.

$$x_0(t) = x_0(0) \exp(-c_0 t) \quad (4.9)$$

where  $c_0$  is a constant proportional to the cross-section  $\sigma_{\text{nAu}}$  of neutron absorption by  ${}^{197}_{79}\text{Au}$ . This equation is plotted in Fig. 4.3 for illustration;

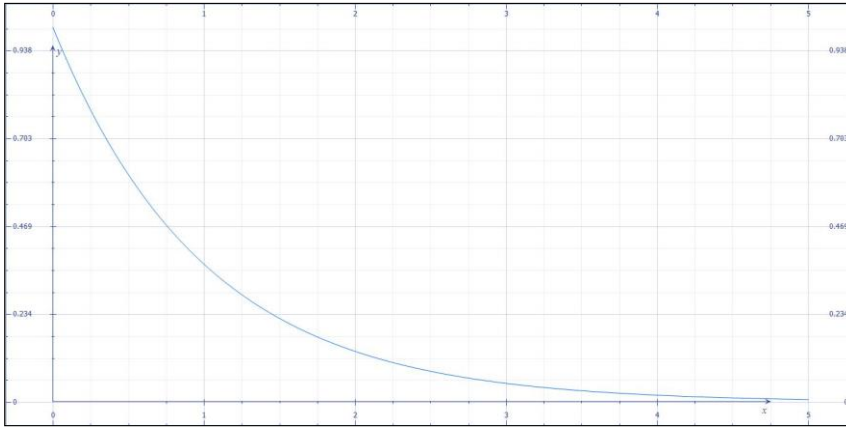


Fig. 4.3 Decrease of the number of gold nucleus  ${}^{197}_{79}\text{Au}$  due to the reaction (4.7).

Then, the next heavier isotope  ${}^{199}_{80}\text{Hg}$  is produced from  ${}^{198}_{80}\text{Hg}$  by the Eq. (4.7) from  ${}^{197}_{79}\text{Au}$  with a rather small cross section  $\sigma_{\text{nHg}}^{(198)} \sim 0.02$  barn tabulated in Table 4.5. The next process from  ${}^{199}_{80}\text{Hg}$  to  ${}^{200}_{80}\text{Hg}$  occurs very fast compared to the former process by the large value of  $\sigma_{\text{nHg}}^{(199)} \sim 2000$  barn. While the next step from  ${}^{200}_{80}\text{Hg}$  to  ${}^{201}_{80}\text{Hg}$  is

slower by the smaller cross section of  $\sigma_{\text{nHg}}^{(200)} < 60$  barn.

Table 4.5 Absorption cross-sections  $\sigma_{\text{nHg}}^{(A)}$  (in barns) of a neutron by mercury isotopes  ${}^A_{80}\text{Hg}$ .

Nucleon number A	196	198	199	200	201	202	204
Neutron absorption cross-section $\sigma_{\text{nHg}}^{(A)}$	(3100)	(0.02)	(2000)	(<60)	(<60)	(4.9)	(0.43)

This story gives a qualitative explanation of the accumulation of  ${}^{198}_{80}\text{Hg}$  and  ${}^{200}_{80}\text{Hg}$  suggesting also applicability of the TNCF model with the mechanism of single-neutron absorption. To show the process a little more quantitatively, we can calculate the process as follows. This process is simulated by model simultaneous equations for variables  $x_i$  written down as follows with tentative values of  $c_i$ ;  $c_0 \sim c_2 > c_1, c_3$ ;

$$dx_0(t)/dt = -c_0 x_0(t), \quad (4.10)$$

$$dx_i(t)/dt = c_{i-1} x_{i-1}(t) - c_i x_i(t) \quad (i = 1 - 3), \quad (4.11)$$

with initial conditions;

$$x_0(0) = x_0^{(0)}, x_i(0) = 0 \quad (i = 1 - 3). \quad (4.12)$$

The solutions for  $x_i$  ( $i = 0 - 3$ ) with constants  $x_0^{(0)} = 10,000$ ,  $c_0 = 100$ ,  $c_1 = 0.01$ ,  $c_2 = 2000$ , and  $c_3 = 60$  are plotted in Fig. 4.4 in semi-logarithmic scale.

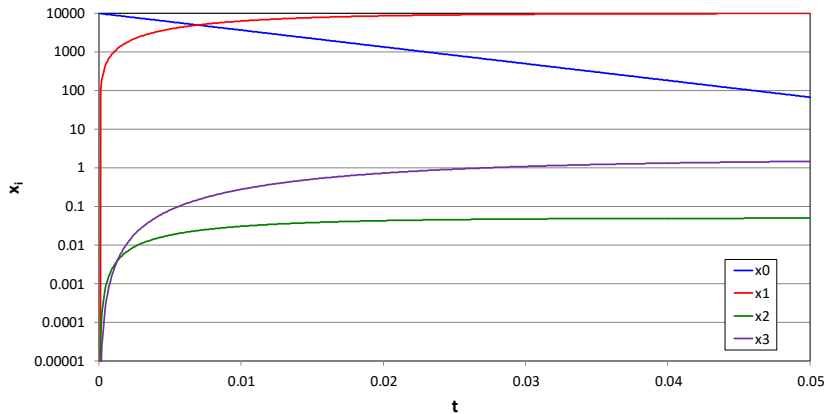


Fig. 4.4 Evolution of density  $x_0$  of  ${}^{197}_{79}\text{Au}$  and  $x_i$  ( $i = 1 - 3$ ) of mercury isotopes  ${}^A_{80}\text{Hg}$  ( $A = 198 - 200$ , respectively) transmuted by neutron absorption according to the equations (4.7) and (4.8).

The results of the tentative calculation using only a single neutron participation given in Fig. 4.4 ( $x_1 > x_3 > x_2$ )<sub>th</sub> with parameters taken rather arbitrary duplicate qualitatively the experimental results shown in Table 4.4 ( $x_3 > x_1 > x_2$ )<sub>ex</sub>, even if the

order of  $x_1$  and  $x_3$  is reversed and suggest applicability of the TNCF model in this case again.

### 4.3 Some Characteristics of the Cathodes with Positive Results

In this section, we want to discuss some minor problems which were not taken up in the above sections. The first is the know-how that is used by experimentalists who performed positive experiments for long years. The second is topographical change of CF materials, another evidence of localization of reactions generating the nuclear transmutation. The third is experimental evidence of development of the CF-matter revealed by the extensive experiments performed by Ohmori et al.

We can boldly speculate on the origin of the two types of CF-matter, type-I and type-II, in relation to the simulation on the neutron star matter [Negele 1973]. Increase of the density  $n_b$  of the neutron star matter results in increase of the number of neutron drops and density of the background neutron-proton medium as shown in Fig. 3.5 of [Kozima 2006a]. It means that the CF-matter is mainly composed of the background neutron-proton medium in the range where  $n_b$  is low (type-I CF-matter) while the number of neutron drops in the CF-matter increases higher where  $n_b$  becomes higher (type-II CF-matter). In the former case, interaction between the CF-matter and a nucleus  $X$  may be governed only by  $n - X$  interaction, while in the latter case it may be governed mainly by  ${}^A_Z\Delta - X$  interaction.

Similar situation is replicated in the experiments with 5d transition-metal cathodes (especially with Au cathode) where the increase of electrolyzing current density  $i$  corresponds to increase of the density  $n_b$  of the neutron star matter. Experimental data shows that increase of the density  $i$  is accompanied by shift of the nuclear transmutation from NT of the 1<sup>st</sup> kind (NT I) to that of the 2<sup>nd</sup> kind (NT II).

#### 4.3.1 Mechanical treatment – A knowhow to realize the CFP

It is necessary to give a mention on the so-called know-how of CF experiment. There are too many discussions on the reproducibility of CF experiments, and opponents used the lack of quantitative reproducibility to denounce the reality of the CFP.

We have known that there is the know-how in each experimenter to perform their experiments successfully. From scarce experience of the author, here is introduced know-how used by experimentalists who performed successful experiments for a long year.

“The electrode surface was scraped with a cleaned glass fragment in order to make crystallographically distorted surface.” [Ohmori 1998b (p. 36 Experimental)]

“One is untreated Pd sheet and the other is cold worked Pd sheet prepared by way of scraping its surface with a cleaned Pyrex-glass fragment.” [Ohmori 2004 (p. 36 Introduction)]

“The palladium foil was scratched on the surface, and the area of the scratch was photographed (Fig. 1a).” [Silver 1993 (p. 423 Experimental Methods and Results)]

“Experiments have been performed using titanium cathodes with various amounts of deformation by cold rolling, which increased the amount of lattice disorder and stress in the cathodes.” [Warner 2000 (p. 161, Experimental Methods and Results)]

### 4.3.2 Topographical change of cathode surface

It is well known that there appears complex surface structures with hills, holes and craters showing melting of the cathode material. A typical figure obtained in an Au cathode is shown in Fig. 2.1 [Ohmori 1997b].

### 4.3.3 Development of the superlattice structure in the CF materials

In Sec. 4.1, we discussed the fulfillment of the necessary condition 2 in the process of electrolysis. The elaborate experiments in the Au/H<sub>2</sub>O/Pt system by Ohmori et al., we can observe another feature of the superlattice formation in the CF material.

In Fig. 4.5, we show the excess heat (W) per unit surface area for Au cathodes; (a) with three kinds of electrolytes Na<sub>2</sub>SO<sub>4</sub>, K<sub>2</sub>SO<sub>4</sub> and K<sub>2</sub>CO<sub>3</sub>, and (b) Excess energy (W) per 5 cm<sup>2</sup> surface area of Au cathode vs. current density (A/cm<sup>2</sup>).

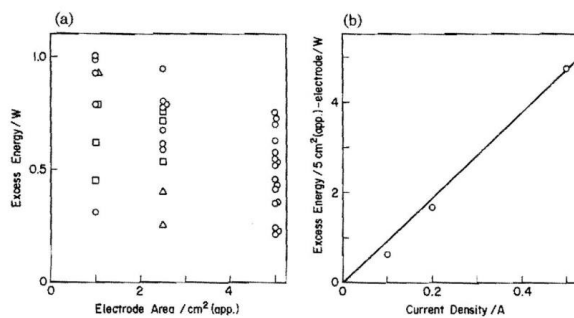


Fig. 5  
Excess energies on various gold electrodes: (a) Plots of the excess energies against the electrode area, (○) Na<sub>2</sub>SO<sub>4</sub> (△) K<sub>2</sub>SO<sub>4</sub> (□) K<sub>2</sub>CO<sub>3</sub>; (b) Plots of the excess energies expressed in unit per 5 cm<sup>2</sup> of the electrode against current density. Current density is referred to the true unit area of the electrode.

Fig. 4.5 (a) Excess energy (W) vs. area of Au cathode and (b) excess energy (W) vs. current density (A/cm<sup>2</sup>) [Ohmori 2000a (Fig. 5)].

In these figures, we see the increase of the superlattice in proportion to the supply of protium (proportional to the current density). We can make an image of superlattice formation in the surface layer of the Au cathode: (1) When protium is supplied to the cathode by electrolysis, protons enter into surface layer of gold at random while its density is low, (2) Increasing the density of proton, there appear islands of superlattice AuH with its total volume proportional to the absorbed protium, (3) Increasing the density of proton further, the volume (or area over the surface) of the superlattice increases by development of individual island or by coalition of islands, (4) Finally, the whole surface of the Au cathode is saturated by the superlattice. The curve in Fig. 4.5 (b) will be saturated in the right with increasing the current density, if the condition of the electrolysis remains the same.

In this point, it should be noticed further the local nature of the superlattice formation as time goes by. Inhomogeneous distribution of islands of the superlattice over the surface, as imagined above, results in the local nature of nuclear reactions in the CFP. As we have discussed often, it is well known in CF research that nuclear reactions in the CFP occur in some localized areas in a surface layer with a width about a few hundred Å [Kozima 2011]. This characteristic is also observed in Au/H<sub>2</sub>O/Pt system as distribution profiles of Fe atoms [Ohmori 1996a] and also as local topographical changes as shown in Fig. 4.3 [Ohmori 1996c].

Here should be noticed another characteristic of the CFP in electrolytic system. The characteristic shown in Fig. 4.4 (a) reveals dependence of the CFP on the electrolyte used in experiments. As have been discussed before [Kozima 2000], there is an interesting favorable combination of cathode metal and electrolyte such as Pd-Li and Ni-K. This favorable combination of cathode-electrolyte seems purely chemical compatibility, but not well explored yet. A scrutinized investigation of the relation shown in Fig. 4.4 (a) may give a clue for the explanation of this problem.

It should be noticed further that the electrolyte plays an essential role in the CFP. One of the most important examples is the production of helium in Pd/D<sub>2</sub>O + LiOH/Pt systems. The data of helium production observed in the Pd cathode [Morrey 1990] has been analyzed and explained semi-quantitatively in consistent with its excess heat data using the reaction;



between a trapped neutron and a lithium nucleus <sup>6</sup>Li absorbed into the Pd cathode from



#### 4.5 On the single neutron absorption in the nuclear transmutation

In Sec. 4.2.1 (b3), we have given an explanation of the production of Re isotopes from W cathode using the single neutron absorption followed by beta decay. Similar explanations for the products of nuclear transmutations in the CFP have given rather quantitatively. Two of such examples are given in Appendix C7 of our book [Kozima 2006]. There, the data by Dash et al. [Klopfenstein 1998, Dash 1996] are analyzed by the TNCF model and the experimental results on the isotopic abundances of Ti and Pd are quantitatively explained by the reactions similar to that given in Eq. (3.1).

In these cases, we used the cross-section  $\sigma_{nX}$  of neutron absorption by a nucleus X determined in nuclear physics. In the above explanation of Re production from W in Sec. 4.2.1 (b3), the data have shown the abundance of the original W reflects directly in the abundance of the product Re without knowledge of the absorption cross-section  $\sigma_{nW}$ . We do not know exactly why there is such difference in two cases; (a) Ti and Pd in normal electrolysis and (b) W in supra-critical electrolysis.

One factor we can imagine is the state of the CF-matter in these two cases. In the case (a), there are only nuclear transmutations with sifts of isotope abundance. While, in the case (b), there are more nuclear transmutations, and we need to use the neutron drops to explain them. In the latter case, it seems the CF-matter is rather turbulent and the reaction where a nucleus reacts with a neutron becomes a part of many-particle reactions including the absorption of a neutron drop (4.3) and transformation of a neutron drop into a nuclide (4.2).

The nuclear transmutation observed in palladium-protium and such hydrogen non-occlusive metals at room temperature as graphite and 5d elements (tungsten, rhenium, gold and platinum) with critical and supra-critical electrolysis are explained by the TNCF model consistently with those observed in 3d and 4d transition-metal hydrides and deuterides with normal electrolysis and also with those observed in XLPE and in biological microbial cultures [Kozima 2016d].

Necessity of critical and supra-critical electrolysis for the CFP in Pd-H system and hydrogen non-occlusive metals seems to heat the samples (CF materials) to higher temperature enough for high proton/deuteron diffusibility and therefore for large extension of wavefunctions of proton/deuteron in the materials [Kozima 2009]. This fact is consistent with the observation of the CFP in PdD rather than PdH systems in relation to the higher diffusivity of D over H at near room temperatures (cf. Appendix A, Fig. A3).

The effect of the nuclear force between a neutron in a lattice nucleus and an interstitial proton/deuteron resulting in the neutron energy band in the case of the CFP is

discussed in Appendix B in relation to the hydrogen diffusion in transition metal hydride.

## 5. Conclusion

The nuclear transmutation observed in CF materials such as palladium-protium and hydrogen non-occlusive metals at room temperature as graphite and 5d elements (W, Re, Au and Pt) with critical and supra-critical electrolysis in electrolytic liquids of light water are explained by the TNCF model consistently with those observed in 3d and 4d transition-metal hydrides and deuterides with normal electrolysis and also with those observed in XLPE and in biological microbial cultures [Kozima 2016d].

Necessity of critical and supra-critical electrolysis for the CFP in Pd-H system and hydrogen non-occlusive metals at around room temperature seems to heat the samples (CF materials) to high temperature enough for high proton/deuteron diffusibility and therefore for large extension of wavefunctions of proton/deuteron in the materials [Kozima 2009].

The success in analysis of the experimental data obtained in graphite and 5d-transition metals, containing a lot of hydrogen, given in this paper has shown the reality of the nuclear transmutations catalyzed by neutrons in CF materials. It is also suggesting the reality of the neutron energy bands in these CF materials realized by the super-nuclear interaction mediated by interstitial protons/deuterons proposed by one of the present author (H.K.).

The super-nuclear interaction between lattice nuclei mediated by interstitial protons/deuterons shows in return a possible interaction between interstitial protons/deuterons mediated by lattice nuclei. This interaction may be called the super p-p (super d-d) interaction for convenience of discussion. Details of this interaction and its effects on the solid state physics will be given in Appendix B.

Thus, the extension of occluded proton/deuteron wavefunctions at an interstitial site  $\mathbf{r}_j$  until lattice points ( $\mathbf{R}_i$ 's) surrounding  $\mathbf{r}_j$  and therefore the nuclear force between the proton/deuteron and a neutron in one of lattice nuclei at  $\mathbf{R}_i$ 's seem to have effect on nuclear physics of the transition metal hydrides/deuterides to induce the CFP on one hand and on solid state physics to induce peculiarity of characteristic diffusivity of hydrogen/deuterium in them on the other.

The effect of the CF-matter on the nuclear physics is characterized by occurrence of nuclear reactions in the transition metal hydrides/deuterides at near room temperature environment which is called by us the cold fusion phenomenon (CFP) to distinguish the phenomenon from other phenomena caused by the nuclear force between particles in the

system discussed in solid state-nuclear physics. The nuclear reactions in the CFP are realized by the interaction between disordered nuclei and trapped neutrons (neutrons in neutron bands) and therefore occur only when there is a near ideal superlattice of lattice nuclei and occluded hydrogen/deuterium (with a large density of occluded hydrogen, i.e.  $H/Me \sim 1$ ).

On the other hand, the effect of the super p-p/d-d interaction on the solid state physics seems to occur even when the density of occluded hydrogen/deuterium is not large as in the case of the diffusion of hydrogen in Pd/Ag alloys as shown in Appendix B. This is because of the large density of lattice nuclei that influence the behavior of hydrogen isotopes. We can expect other examples of the effect of the super p-p/d-d interaction on the hydrogen/deuterium behavior in the solid state physics at higher concentrations. This point is a theme of future investigation.

## **Appendix A. Hydrogen isotopes in Metals**

[Birnbaum 1972, Sussmann 1972, Springer 1978, Wicke 1978, Voelkl 1978, Puska 1984, Fukai 2005, Kozima 2006 (Sec. 3.6), Griessen 2008]

[Griessen 2008]

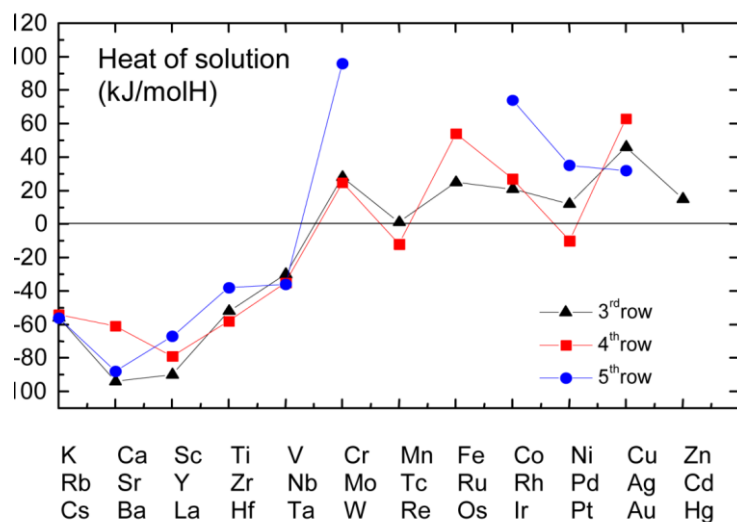


Fig. A1 Heat of solution of hydrogen in the rows of the periodic system which contains the 3d, 4d and 5d elements. For references see Griessen and Riesterer<sup>15</sup>. [Griessen 2008 (Fig. III.15)]

15. Griessen, R., and T. Riesterer, "Heat of formation models" in Topics in Applied Physics **63** (1988) 219, Springer-Verlag

The data shown in Fig. A1 tells us the high values of heat of solution for the 5d elements (W, Re, Pt and Au) used in the CF experiments introduced in Sec. 2. This thermodynamic data is the cause of high temperature to realize the CFP in them by the critical and supra-critical electrolysis.

Table A1 Heat of solution of hydrogen in the elements of the periodic system [Giessen 2008 (Table III.1)]

Element	Enthalpy of solution (kJ/molH)	Enthalpy of solution (eV/atom)
He	--	--
Li	-51	-0.528
Be	-2	-0.02
B	-4	-0.041
C	--	--
N	--	--
O	--	--
F	--	--
Ne	--	--
Na	2	0.02
Mg	21	0.217
Al	60	0.621
Si	180	1.865
P	--	--
S	--	--
Cl	--	--
Ar	--	--
K	0	0
Ca	-94	-0.974
Sc	-90	-0.932
Ti	-52	-0.538
V	-30	-0.31
Cr	28	0.29
Mn	1	0.01
Fe	25	0.259
Co	21	0.217
Ni	12	0.124
Cu	46	0.476
Zn	15	0.155
Ga	--	--
Ge	221	2.29
As	--	--
Se	35	0.362
Br	--	--
Kr	--	--
Rb	-54	-0.559
Sr	-61	-0.632
Y	-79	-0.818
Zr	-58	-0.601
Nb	-35	-0.362
Mo	25	0.259
Tc	-12	-0.124
Ru	54	0.559
Rh	27	0.279
Pd	-10	-0.103

Element	Enthalpy of solution (kJ/molH)	Enthalpy of solution (eV/atom)
Ag	63	0.652
Cd	-94	-0.974
In	--	--
Sn	125	1.295
Sb	--	--
Te	-84	-0.87
I	--	--
Xe	--	--
Cs	-56	-0.58
Ba	-88	-0.912
La	-67	-0.694
Ce	-74	-0.766
Pr	-68	-0.704
Nd	-50	-0.518
Pm	--	--
Sm	-70	-0.725
Eu	--	--
Gd	-69	-0.715
Tb	-78	-0.808
Dy	-79	-0.818
Ho	--	--
Er	--	--
Tm	--	--
Yb	--	--
Lu	-79	-0.818
Hf	-38	-0.393
Ta	-36	-0.373
W	96	0.994
Re	--	--
Os	--	--
Ir	74	0.766
Pt	35	0.362
Au	32	0.331
Hg	--	--
Tl	--	--
Pb	62	0.642
Bi	--	--
Po	--	--
At	--	--
Rn	--	--
Fr	--	--
Ra	--	--
Ac	--	--
Th	-40	-0.414
Pa	--	--
U	7	0.072



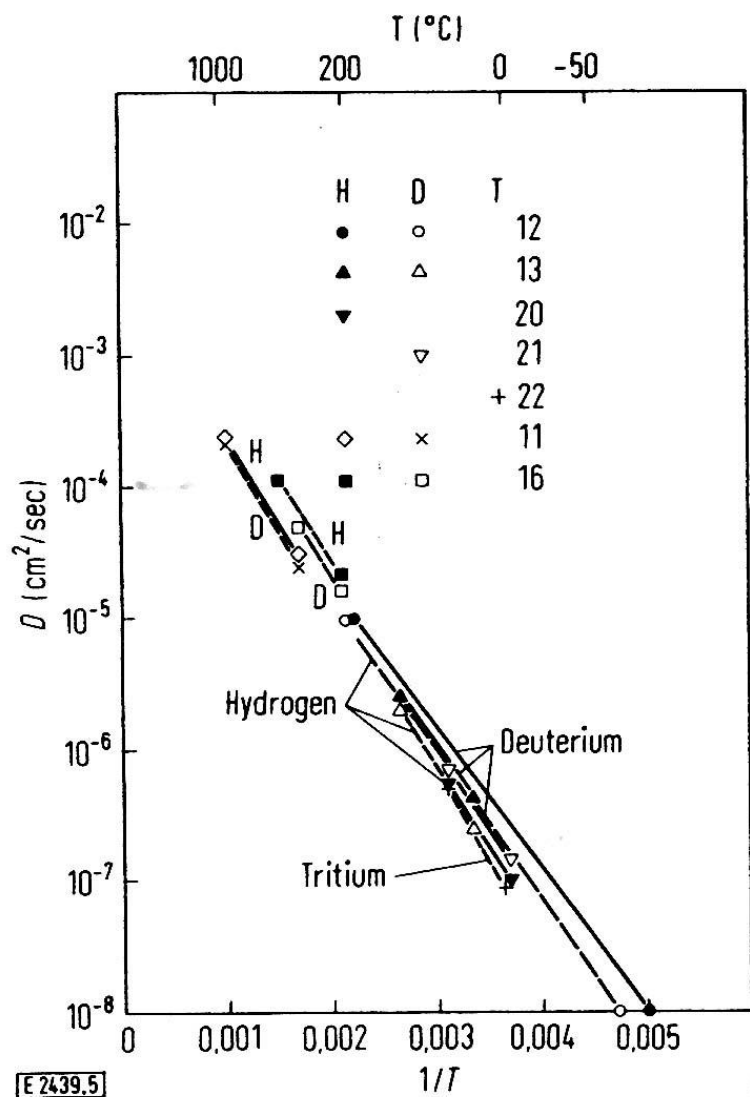


Fig. A3 Diffusion of isotopes in palladium [Birbaum 1972 (Fig. 5)]

H and D diffusion in Pd [Kozima 1998, 2006, 2013a, 2014a, 2016] D has higher diffusibility at room temperature than H while at higher temperatures above 200 °C the situation reverses. This is the reason for the critical electrolysis for Pd-H system to realize the CFP compared to the normal electrolysis for Pd-D system usually performed in CF experiments [Fleischmann 1989, McKubre 1991] It should be remembered that

there have been successful experiments observing the CFP in Pd-H<sub>2</sub>O system at normal electrolysis with a little higher current densities (e.g. [Dash 1994]).

It is interesting to know that Martin Fleischmann noticed this fact shown in Fig. A3 already in 1990 from his point of view as follows;

“Such calculations must also provide answers to other conundrums such as why the diffusion coefficient of D in Pd/D exceeds those of both H in Pd/H and T in Pd/T.” [Fleischmann 1990 (p. 347)]

Experiments on the graphite electrodes at arc discharge (e.g. [Hanawa 2000]) was analyzed in our paper [Kozima 2016b].

It is interesting to notice that hydrogen isotopes have low diffusivity, which is the reason the supra-critical electrolysis is necessary as done by Ohmori et al. The data of H and D in Re, Pt, W and Au are given by [Birnbaum 1972, Fukai 2005 (Tables 5.4, 5.10, Figure 5.49)]. H or D have lower diffusivity in Re, Pt and W than in Pd. It means higher temperature is necessary to have the extended wavefunctions of excited states of H and D in these metals. (No data in Au)

#### **H/D in W, Re and Pt**

The vibrational excitation energy of interstitial hydrogen in rhenium (Re) is shown in Table A2 ([Fukai 2005 (Table 5.4)]). The excitation energy of hydrogen in Re (~ 100, 130 meV at 5 K in ReH<sub>0.09</sub>) is compared with that in Pd ~ 56.0 meV at 15 K in PdH<sub>0.99</sub> and ~ 69.0 meV at 77 K in PdH<sub>0.002</sub> (Table not shown here). The rather high value of the excitation energy in Re tells us the lower diffusivity of hydrogen isotopes in Re than that in Pd which is a typical metal for the high diffusivity of hydrogen.

The binding energy of hydrogen atoms with monovacancies in tungsten (W) is shown in Table A2 ([Fukai 2005 (Table 5.10)]). The large value of the binding energy of proton and vacancy in W (1.43 eV) tells us indirectly that the proton in W is in a rather stable state than that in Pd where the binding energy is lower (0.23, 0.15 eV).

Table A2 Vibrational excitation energies of interstitial hydrogen in metals. The values have been obtained from the observed peaks of inelastic neutron scattering experiments using polycrystalline (powder) specimens. The presence of dispersion in fcc and some hcp metals detracts to some extent from the physical significance of these values. [Fukai 2005 (Table 5.4)]

**Table 5.4.** (*continued*)

Structure	Site	Sample	Excitation Energy [meV]		Temperature [K]	Reference
bct	O	VH <sub>0.5</sub>	50.2 <sup>a</sup>	223 <sup>b</sup>	80	[5.59]
			56	230	80	[5.72]
			54	220	295	[5.72]
		VD <sub>0.5</sub>	39	164	80	[5.72]
			47		295	[5.72]
		VT <sub>0.5</sub>	36		295	[5.72]
bcc	T	TiH <sub>0.14</sub>	120(2) <sup>b</sup>	171(2) <sup>a</sup>	998	[5.73]
		VH <sub>0.012</sub>	106	~170	300	[5.58]
		VH <sub>0.51</sub>	113	180	498	[5.74]
		VD <sub>0.5</sub>	82(3)	123(7)	425	[5.75]
		NbH <sub>0.03</sub>	107	163	300	[5.58]
		NbH <sub>0.7</sub>	116.0(7)	167.0(15)	10	[5.76]
		NbD <sub>0.85</sub>	86(1)	120.0(15)	10	[5.76]
		NbT <sub>0.7</sub>	72(1)	101(1)	10	[5.76]
		TaH <sub>0.037</sub>	114	154	300	[5.58]
		TaH <sub>0.08</sub>	114.0(6)	163.5(8)	300	[5.77]
		TaH <sub>0.5</sub>	121.3(2)	163.4(4)	10	[5.76]
		TaD <sub>0.09</sub>	84.4(6)	116.0(6)	300	[5.77]
		TaD <sub>0.5</sub>	88.4(4)	118.7(6)	10	[5.76]
hcp	O	CrH <sub>1.0</sub>	121		15	[5.53]
		MnH <sub>0.86</sub>	111		100	[5.51]
		FeH <sub>1.0</sub> <sup>c</sup>	105		90	[5.78]
		CoH <sub>0.05</sub>	118		5	[5.65]
		CoH <sub>0.5</sub>	110		15	[5.65]
		MoH <sub>1.2</sub>	113		15	[5.53]
		ReH <sub>0.09</sub>	100, 130		5	[5.63]
hcp	T	ScH <sub>0.34</sub> <sup>d</sup>	103.5(2) <sup>b</sup>	147.5(1) <sup>a</sup>	8	[5.60]
		ScD <sub>0.34</sub> <sup>d</sup>	79.0(1)	107.3(1)	4	[5.60]
		YH <sub>0.18</sub> <sup>d</sup>	100.1(2)	134.2(5)	80	[2.133]
		YD <sub>0.18</sub> <sup>d</sup>	75.8(1)	96.3(1)	80	[2.133]
		LuH <sub>0.19</sub> <sup>d</sup>	102.8(3)	143.5(1)	4	[5.62]
		LuD <sub>0.19</sub> <sup>d</sup>	76.2(1)	101.7(1)	4	[5.62]
		TiH <sub>0.05</sub>		141(1)	588	[5.73]
		TiH <sub>0.07</sub>	105.5(20)	162.0(25)	599	[5.79]
		TiD <sub>0.09</sub>		108.4(12)	601	[5.79]
		ZrH <sub>0.05</sub>		143.1(6)	873	[5.79]
		ZrD <sub>0.05</sub>		105.0(10)	765	[5.79]

<sup>a</sup> doubly degenerate mode

<sup>b</sup> non-degenerate mode

<sup>c</sup> dhcp structure

<sup>d</sup> single-crystal data.

Table A3 Binding energies of hydrogen atoms with monovacancies and bubbles/voids, obtained by various methods; including ion implantation/channeling (I/C), positron annihilation spectroscopy (PAAS), superabundant vacancy formation/thermal desorption spectroscopy (SAV/TDS). All energies are in eV. [Fukai 2005 (Table 5.10)]

Metal	Vacancy	Bubble/Void	Method	Reference
Al	~0.52	≤0.52	I/C	[5.176]
	0.53		PAS	[5.148]
V	0.11		I/C	[5.177]
	0.23		I/C	[5.19]
Cr	0.89, 0.73		SAV/TDS	[4.44]
Fe	0.63, 0.43	0.78	I/C	[5.175]
Ni	0.44, 0.28	0.55	I/C	[5.163]
	0.58		PAS	[5.149]
	0.44		PAS	[5.150]
	0.43, 0.27		SAV/TDS	[5.178]
	0.45, 0.28		SAV/TDS	[5.179]
Cu	0.42, 0.22		I/C	[5.167]
	0.37, 0.23		SAV/TDS	[5.179]
Zr	0.28		I/C	[5.180]
Nb	0.55		PAS	[5.144, 5.145]
Mo	1.03, 0.80	1.15	I/C	[5.176]
	1.4		PAS	[5.149]
Pd	0.23, 0.15	0.31	I/C	[5.153, 5.181]
Ta	0.58		PAS	[5.145]
	0.42		I/C	[5.182]
W	1.43	0.53	I/C	[5.183]

Diffusion data of hydrogen in tungsten at higher temperature from 1100 to 2600 K is given in Table A4 ([Birnbbaum 1972]). There is no data of tungsten diffusion at lower temperatures.

The data in Table A2 and A3 tell us that hydrogen is not occluded in tungsten at lower temperatures.

Table A4. Hydrogen diffusion data at elevated temperatures – bcc metals. [Birnbaum 1972 (Table 5)].

Metal	$D_0$ (cm <sup>2</sup> /sec)	$Q$ (kcal/mol)	Temperature Range (°K)	Method Ref.
Nb	$2.2 \cdot 10^{-2}$	9.37	575 – 975	Absorption [26]
	$1.8 \cdot 10^{-2}$	10.0	475 – 975	Absorption [27]
	$5.6 \cdot 10^{-2}$	19.2	1875 – 2575	Desorption [43]
$\alpha$ -Fe	$7.6 \cdot 10^{-4}$	2.3	675 – 1175	Permeability [28]
	$2.2 \cdot 10^{-3}$	2.9	675 – 1175	Permeability [29]
	$5.3 \cdot 10^{-3}$	3.05	425 – 1175	Desorption [30]
	$9.3 \cdot 10^{-4}$	2.7	475 – 1050	Desorption [31]
	$1.4 \cdot 10^{-3}$	3.2	475 – 1050	Desorption [32]
	$6.4 \cdot 10^{-4}$	1.92	575 – 1050	Desorption [9]
	$6.4 \cdot 10^{-4}$	1.33	283 – 350	Permeability [33]
	$2.2 \cdot 10^{-3}$	3.1	283 – 373	Desorption [34]
Ta	$6.1 \cdot 10^{-4}$	3.5	273 – 435	Resistivity [35]
	$7.5 \cdot 10^{-2}$	14.4	675 – 800	Permeability [41]
	$1.6 \cdot 10^{-3}$	32.2	775 – 975	Absorption [42]
	$6.5 \cdot 10^{-4}$	3.5	300 – 360	Lattice Expansion [79]
Mo	$7.6 \cdot 10^{-5}$	8.4	525 – 625	Permeability [37]
	$5.9 \cdot 10^{-2}$	14.7	875 – 1275	Desorption [38]
	$1.6 \cdot 10^{-1}$	22.2	1875 – 2575	Desorption [39]
W	$4.1 \cdot 10^{-3}$	9.0	1100 – 2400	Permeability [36]
	$8.1 \cdot 10^{-2}$	19.8	1900 – 2600	Desorption [42]
	$7.3 \cdot 10^{-4}$	41.5	1975 – 2200	Thermal Dissociation [40]

Change in the lattice location of D atoms implanted in Pt at low temperatures upon subsequent annealing is shown in Fig. A4. [Fukai 2005 (Fig. 5.49)] This data tells us that deuterium in Pt with  $T_D \sim 100$  K is more stable than that in Pd with  $T_D \sim 85$  K. This might be the reason that hydrogen isotopes are diffusive in Pd but not in Pt at around room temperatures.

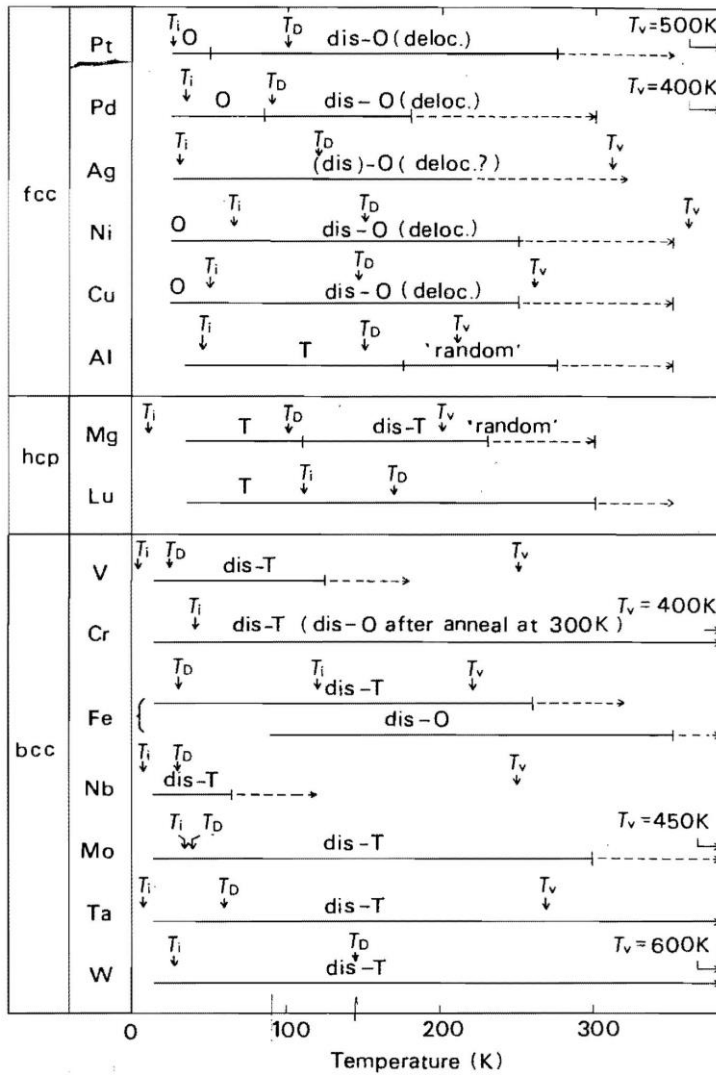


Fig. A4 Changes in the lattice location of D atoms implanted at low temperatures upon subsequent annealing. The temperatures where interstitials, vacancies and D atoms start migrating are designated, respectively, as  $T_i$ ,  $T_v$ , and  $T_D$ . Lu is an exceptional case where  $T_D$  marks the temperature of the break-up of H-M-H pairs (Sec. 5.6.1). For the geometry of displaced-T (dis-T) and displaced-O (dis-O) configurations, see the text. A transition from solid to dashed line marks the temperature at which D atoms are released from the implanted region. For references, see the text. [Fukai 2005 (Fig. 5.49)]

書式変更: フォント : 10.5 pt

書式変更: フォント : 10.5 pt

書式変更: フォント : 10.5 pt, 下付き

## **Appendix B. Nuclear Interaction between Hydrogen/Deuterium and Lattice Nuclei and Super p-p Attractive Interaction in CF Materials**

In the analyses of the cold fusion phenomenon (CFP) observed in the transition metal hydrides/deuterides, we have shown that the nuclear force between a proton/deuteron and a neutron in a lattice nucleus resulted in the super-nuclear interaction between neutrons in lattice nuclei, which has given a unified explanation of whole experimental data obtained in protium and deuterium systems altogether. The nuclear force between a proton/deuteron and a neutron in a lattice nucleus has another phase on the behavior of hydrogen/deuterium in these materials.

A proton/deuteron in an interstitial site with extended wavefunction until neighboring lattice points interacts with neutrons in the lattice nuclei at these lattice points. If the proton/deuteron is at an octahedral interstitial site, there are eight neighbors and the interaction may be fairly large; comparable to or stronger than the short-range force with electrostatic nature in some situations.

Increasing the concentration of occluded hydrogen/deuterium, there appears a situation where two protons/deuterons are in adjacent interstitials and they interact with common lattice nuclei surrounding them. Then, there appears the super p-p/d-d interaction between these two protons/deuterons.

We can illustrate the super p-p (super d-d) interaction in CF materials schematically using PdH crystal in two dimensions in Fig. B1. Let us take up a proton  $j$  at an interstitial site  $j$  and another proton  $k$  at site  $k$  for illustration. We assume that the wavefunctions of these protons at interstitials overlap with lattice nuclei at  $i$  and  $i'$ . The proton  $j$  interacts with the neutrons at  $i$  and  $i'$  with the nuclear force and the proton  $k$  also interacts with these neutrons. Then, the proton  $j$  and proton  $k$  interact with each other through their interactions with neutrons in lattice nuclei at  $i$  and  $i'$ . This interaction of two protons  $j$  and  $k$  mediated by neutrons in lattice nuclei is called the “super p-p interaction.” This situation is illustrated in Fig. B1.

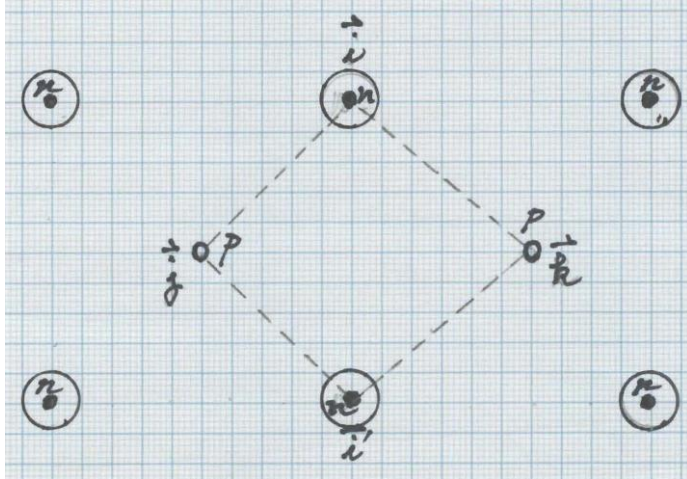


Fig. B1 Schematic illustration of the super p-p interaction between a proton at  $j$  and a proton at  $k$  mediated by neutrons in lattice nuclei  $i$  and  $i'$  in two dimensions.

About the strength of the supposed super p-p/d-d interaction compared to that of the electrostatic interactions among surrounding protons/deuterons and lattice nuclei, we have to calculate it from the first principle or estimate it using experimental data related to this interaction. From the experimental data cited below, we can give a rough comparison between the super p-p interaction with the short-range interaction (between nearest neighbors) of two hydrogens in palladium alloys. There are many unsolved problems in solid state physics of transition metal hydrides with known interactions as shown below. The existence of this super p-p/d-d interaction may give a light to solve these problems, if the effect of the former interaction on the behavior of protons/deuterons in solid state physics seems fairly large with the same order of magnitude to that of the latter.

One of excellent reviews on the physics of hydrogen in palladium and palladium alloys has been given by Wicke and Brodowsky [Wicke 1978]. In this review, the fundamental problem of the physics of Pd-H (D) systems is explained as follows:

“Nevertheless, there are quite a number of details in the mechanism of hydrogen diffusion as well as in the behavior of detailed electronic states in this system not yet fully understood. - - -”

“A basic problem still in discussion is which type of model will be most adequate for handling the attractive hydrogen-hydrogen interactions induced by the elastic strains of the host lattice. In one type of model, particular emphasis is laid upon the long-range

part of these interactions, and it is suggested that short-range attractions do not occur, i.e., that the short-range interactions are purely repulsive.”

“Macroscopic elasticity theory is involved in this model, and mean-field approximations are used; the statistics are rather cumbersome, if the simple Bragg-Williams approximation is not applied. The other type of model is based upon short-range attractive interaction, acting predominantly between nearest neighbors, such that the concept of pair interaction and the statistical method of the quasichemical approximation can be applied. - - - The real condition will be somewhere intermediate, as often in nature, between the two simplifying concepts of short-range and of long-range interactions, but the full treatment of the general case is still lacking.” [Wicke 1978 (pp. 73 – 74)] (Underlined at citation).

This explanation on the nature of the hydrogen-hydrogen interaction suggests us that the super p-p interaction explained above with an intermediate-range character may give a possibility to explain the physics of hydrogen diffusion in palladium and palladium alloys.

To investigate possible effects of the super p-p/d-d interaction on the physics of transition metal hydrides/deuterides, we take up two examples below.

- (1) First example is the hydrogen diffusion in Pd/Ag alloys. Figures B2 and B3 show diffusion coefficients of H in Pd/Ag alloys as functions of hydrogen potential  $\eta$  (proportional to the logarithm of  $H_2$  pressure, which is a function of  $n$  ( $=H/Me$ ), in the case of a film penetration experiment) and atomic ratio  $n$ , respectively.

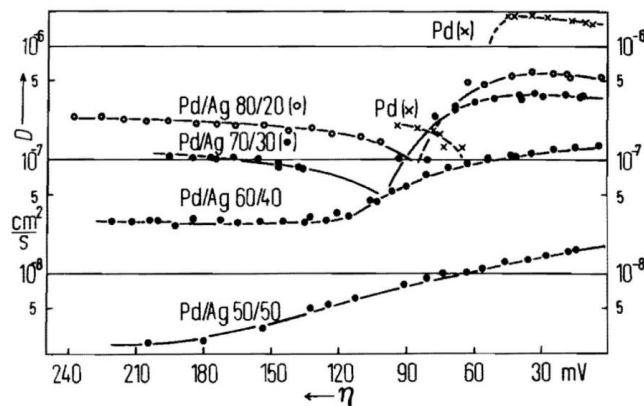


Fig. B2. Plots of diffusion coefficients of H in Pd/Ag alloys vs. hydrogen potential  $\eta$  (proportional to the logarithm of  $H_2$  pressure) at 30 °C. [Wicke 1978 (Fig. 3.33)]

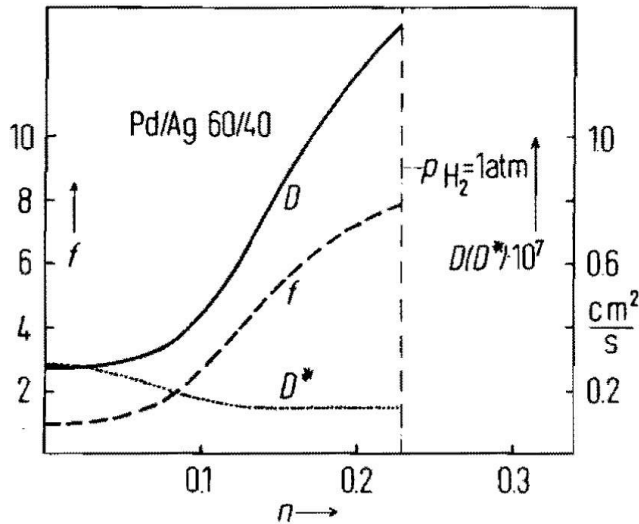


Fig. B3. Dependence of Fick's ( $D$ ) and Einstein's ( $D^*$ ) diffusion coefficients and of the thermodynamic factor  $f$  on atomic ratio H/Me ( $= n$ ). [Wicke 1978 (Fig. 3.34)]

The data is not fully understood yet as it is explained in their text as follows:

“The decrease of  $D^*$  with increasing  $n$  can be attributed partly to the vacancy factor ( $1 - n$ ); the residual influence of concentration on  $D^*$  has not been explained so far.” [Wicke 1978 (p. 148)]

If we can imagine that there is the attractive super p-p interaction between protons in Pd/Ag alloys, diffusion is disturbed by this interaction in proportion to the density  $n$  of the protons in the lattice in accordance with the experimental data.

(2) The second example is the influence of alloy components on the mobility of hydrogen in alloys  $Pd_{1-x}Me_x$  ( $Me = Ag, Au, Ni, \text{ and } Pt$ ). The problem is explained by Wicke as follows:

“The influence of alloy components on the mobility of hydrogen in Pd is remarkably small at low additions. Ag, Au, Ni, and Pt up to about 25 at.% leave the diffusion coefficient and the activation energy nearly unchanged. At higher additions the activation energies increase and the diffusion constants decline in a nearly logarithmic fashion to quite low values for alloys with 50 or 60 at.% of solute.” [Wicke 1978 (p. 150)] (Underlined at citation).

This interesting behavior of mobility of hydrogen at low concentrations of several minor components (Ag, Au, Ni, and Pt) up to about 25 % may reveal existence of a

force other than the short-range force between nearest neighbors H and Pd or H and Me. Because the super p-p interaction with an intermediate-range character is not sensitive to the atomic natures of lattice nuclei and also to the small number of minor components, we can expect the same behavior of protons in Pd<sub>1-x</sub>Me<sub>x</sub> alloys (Me = Ag, Au, Ni, and Pt) for small values of x less than 0.25.

## References

- [**Alefeld 1978**] G. Alefeld and J. Voelkl, Introduction, in G. Alefeld, J. Voelkl (eds.): Hydrogen in Metals I, Basic Properties. Topics in Applied Physics, Vol. 28 (Springer, Berlin, Heidelberg, New York 1978), pp. 1 – 4 (1978).
- [**Azumi 1999**] K. Azumi, T. Mizuno, T. Akimoto and T. Ohmori, "Light Emission from Pt during High-Voltage Cathodic Polarization," J. Electrochemical Society, 146 (9), pp. 3374 – 3377 (1999).
- [**Birnbaum 1972**] H.K. Birnbaum and C.A. Wert, "Diffusion of Hydrogen in Metals," Berichte der Bunsen-Gesellschaft, **76** (8), pp. 806 – 816 (1972).
- [**Cirillo 2004**] C. Cirillo, A. Dattilo and V. Iorio; "Transmutation of Metal at Low Energy in a Confined Plasma in Water"; Proc. ICCF11, pp. 492 – 504 (2004), ISBN 981-256-640-6.
- [**Dash 1994**] J. Dash, G. Noble and D. Diman, "Changes in Surface Topography and Microcomposition of a Palladium Cathode caused by Electrolysis in Acidified Light Water," Proc. Int. Symposium on Cold Fusion and Advanced Energy Sources (Minsk, Belarus, May 25 – 26, 1994), pp. 172 – 183 (1994).
- [**Fleischmann 1989**] M. Fleischmann, S. Pons and M. Hawkins, "Electrochemically induced Nuclear Fusion of Deuterium," J. Electroanal. Chem., 261, 301 – 308 (1989), ISSN: 1572-6657.
- [**Fukai 2005**] Y. Fukai, The Metal-Hydrogen System, Springer, 2005, ISBN-10; 3642047211.
- [**Griessen 2008**] Ronald Griessen and Andreas Zuettel, "Chapter III, Thermodynamics of Hydrogen in Metals," in Science and Technology of Hydrogen in Metals, Lecture note at Vrije Universiteit, Amsterdam, 2008, <http://www.nat.vu.nl/~griessen/STofHinM/>
- [**Hanawa 2000**] T. Hanawa, "X-ray Spectrometric Analysis of Carbon Arc Products in Water," Proc. ICCF8, pp. 147 – 152 (2000), ISBN 88-7794-256-8
- [**Kozima 1994**] H. Kozima, "Trapped Neutron Catalyzed Fusion of Deuterons and Protons in Inhomogeneous Solids," Trans. Fusion Technol., **26**, 508 - 515 (1994), ISSN 0748-1896.

**[Kozima 1998]** H. Kozima, *Discovery of the Cold Fusion Phenomenon – Development of Solid State-Nuclear Physics and the Energy Crisis in the 21<sup>st</sup> Century –*, Ohtake Shuppan Inc., 1998, ISBN 4-87186-044-2.

**[Kozima 2000]** H. Kozima, “Electroanalytical Chemistry in Cold Fusion Phenomenon,” in *Recent Research Developments in Electroanalytical Chemistry*, Edited by S.G. Pandalay, Vol. **2**, pp. 35 – 46 (2000), ISBN 81-86846-94-8.

**[Kozima 2006]**, *The Science of the Cold Fusion Phenomenon – In Search of the Physics and Chemistry behind Complex Experimental Data Sets –*, 1<sup>st</sup> Edition, Elsevier, Amsterdam, 2006, ISBN-13: 978-0-08045-110-7, ISBN-10: 0-080-45110-1.

**[Kozima 2008a]** H. Kozima, W.-S. Zhang and J. Dash, “Precision Measurement of Excess Energy in Electrolytic System Pd/D/H<sub>2</sub>SO<sub>4</sub> and Inverse-Power Distribution of Energy Pulses vs. Excess Energy” *Proc. ICCF13*, pp. 348 – 358 (2008), ISBN 978-5-93271-428-7.

**[Kozima 2008b]** H. Kozima, “Physics of the Cold Fusion Phenomenon” *Proc. ICCF13*, pp. 690 – 703 (2008), ISBN 978-5-93271-428-7.

**[Kozima 2009]** H. Kozima, “Non-localized Proton/Deuteron Wavefunctions and Neutron energy bands in Transition-metal Hydrides/Deuterides,” *Proc. JCF9*, pp. 84 – 93 (2009), ISSN 2187-2260. Proceedings of JCF9 is posted at JCF website:

[http://www.jcf.rs.org/proc\\_jcf.html](http://www.jcf.rs.org/proc_jcf.html)

**[Kozima 2011]** H. Kozima, “Localization of Nuclear Reactions in the Cold Fusion Phenomenon,” *Proc. JCF11*, pp. 59 – 69 (2011), ISSN 2187-2260. Proceedings of JCF11 is posted at JCF website: [http://www.jcf.rs.org/proc\\_jcf.html](http://www.jcf.rs.org/proc_jcf.html)

**[Kozima 2012]** H. Kozima and T. Tada, “The Cold Fusion Phenomenon in Hydrogen-graphites,” *Proc. JCF12*, pp. 77 – 92 (2012), ISSN 2187-2260. Proceedings of JCF12 is posted at JCF website: [http://www.jcf.rs.org/proc\\_jcf.html](http://www.jcf.rs.org/proc_jcf.html)

**[Kozima 2013]** H. Kozima, “Cold Fusion Phenomenon in Open, Nonequilibrium, Multicomponent Systems – Self-organization of Optimum Structure,” *Proc. JCF13*, **13-19**, pp. 134 – 157 (2013), ISSN 2187-2260. Proceedings of JCF13 is posted at JCF website: [http://www.jcf.rs.org/proc\\_jcf.html](http://www.jcf.rs.org/proc_jcf.html)

**[Kozima 2014a]** H. Kozima, “Nuclear Transmutations (NTs) in Cold Fusion Phenomenon (CFP) and Nuclear Physics,” *Proc. JCF14*, **14–15**, pp. 168 - 202 (2014). ISSN 2187-2260. Proceedings of JCF14 is posted at JCF website:

[http://www.jcf.rs.org/proc\\_jcf.html](http://www.jcf.rs.org/proc_jcf.html)

**[Kozima 2014b]** H. Kozima, “The Cold Fusion Phenomenon – What is It?” *Proc. JCF14*, **14-16**, pp. 203 – 230 (2014), ISSN 2187-2260. Proceedings of JCF14 is posted at JCF website: [http://www.jcf.rs.org/proc\\_jcf.html](http://www.jcf.rs.org/proc_jcf.html)

- [Kozima 2016a]**, The Science of the Cold Fusion Phenomenon – In Search of the Physics and Chemistry behind Complex Experimental Data Sets –, 2<sup>nd</sup> Edition, Elsevier, Amsterdam, 2016 (to be published). A part of this book is posted at CFRL website prior to publication: <http://www.geocities.jp/hjrfq930/Books/bookse/bookse.html>
- [Kozima 2016b]** H. Kozima, “From the History of CF Research – A Review of the Typical Papers on the Cold Fusion Phenomenon –, Proc. JCF16, **16-13**, pp. 116 – 157 (2016), ISSN 2187-2260. Proceedings of JCF16 is posted at JCF website: [http://www.jcfrs.org/proc\\_jcf.html](http://www.jcfrs.org/proc_jcf.html)
- [Kozima 2016c]** H. Kozima and K. Kaki, “The Cold Fusion Phenomenon and Neutrons in Solids,” Proc. JCF16, **16-14**, 158 – 198 (2016), ISSN 2187-2260. Proceedings of JCF16 is posted at JCF website: [http://www.jcfrs.org/proc\\_jcf.html](http://www.jcfrs.org/proc_jcf.html)
- [Kozima 2016d]** H. Kozima, “Nuclear Transmutations in Polyethylene (XLPE) Films and Water Tree Generation in Them (2),” Proc. JCF16, **16-17**, pp. 210 – 215 (2016), ISSN 2187-2260. Proceedings of JCF16 is posted at JCF website: [http://www.jcfrs.org/proc\\_jcf.html](http://www.jcfrs.org/proc_jcf.html)
- [Kozima 2016e]** H. Kozima, “Biotransmutation as a Cold Fusion Phenomenon,” Proc. JCF16, **16-18**, pp. 216 – 239 (2016), ISSN 2187-2260. Proceedings of JCF16 is posted at JCF website: [http://www.jcfrs.org/proc\\_jcf.html](http://www.jcfrs.org/proc_jcf.html)
- [McKubre 1991]** M.C.H. McKubre, R. Rocha-Filho, S.I. Smedley, F.L. Tanzella, S. Crouch-Baker, T.O. Passell and J. Santucci, “Isothermal Flow Calorimetric Investigations of the D/Pd System,” Proc. ICCF2, pp. 419 – 443 (1991), ISBN 88-7794-045-X.
- [McKubre 1994]** McKubre, M.C.H., et al., Development of Advanced Concepts for Nuclear Processes in Deuterated Metals, TR-104195. 1994, Electric Power Research Institute.
- [Miley 1996a]** G.H. Miley, G. Narne, M.J. Williams, J.A. Patterson, J. Nix, D. Cravens and H. Hora, “Quantitative Observation of Transmutation Products occurring in Thin-film Coated Microspheres during Electrolysis,” Proc. ICCF6 pp. 629 – 644 (1996).
- [Mizuno 1998a]** T. Mizuno, T. Ohmori and T. Akimoto, “Probability of Neutron and Heat Emission from Pt Electrode Induced by Discharge in the Alkaline Solution,” Proc. ICCF7, pp. 247 – 252 (1998), ENECO Inc.
- [Mizuno 1998b]** T. Mizuno, T. Ohmori and T. Akimoto, “Detection of Radiation Emission, Heat Generation and Elements from a Pt Electrode Induced by Electrolytic Discharge in the Alkaline Solution,” Proc. ICCF7, pp. 253 – 258 (1998), ENECO Inc.
- [Mizuno 1998c]** T. Mizuno, T. Akimoto T. Ohmori and M. Enyo, “Confirmation of the

Changes of Isotopic Distribution for the Elements on Palladium Cathode after Strong Electrolysis in D<sub>2</sub>O Solution,” *Int. J. Soc. of Mat. Eng. for Resources*, **6** (1), pp. 45 – 59 (1998).

[**Negele 1973**] J.W. Negele and D. Vautherin, “Neutron Star Matter at Sub-nuclear Densities,” *Nuclear Physics*, **A207**, 298 - 320 (1973).

[**Ohmori 1996a**] T. Ohmori and M. Enyo, “Iron Formation in Gold and Palladium Cathodes,” *J. New Energy*, 1-1, pp. 15 – 19 (1996), ISSN 1086-8259.

[**Ohmori 1996b**] T. Ohmori, T. Mizuno and M. Enyo, “Production of Heavy Metal Elements and the Anomalous Surface Structure of the Electrode Produced during the Light Water Electrolysis on Au Electrode,” *Proc. ICCF6*, pp. 670 – 674 (1996), NEDO and IAE, Japan.

[**Ohmori 1996c**] T. Ohmori, T. Mizuno and M. Enyo, “Isotopic Distributions of Heavy Metal Elements Produced during the Light Water Electrolysis on Au Electrode,” *J. New Energy*, **1-3**, pp. 90– 99 (1996), ISSN 1086-8259.

[**Ohmori 1997a**] T. Ohmori, T. Mizuno, H. Minagawa and M. Enyo, “Low Temperature Nuclear Transmutation forming Iron on/in Gold Electrode during Light Water Electrolysis,” *Int. J. Hydrogen Energy*, **23** (5), pp. 459 – 463 (1997), ISSN 0360-3199.

[**Ohmori 1997b**] T. Ohmori and T. Mizuno, “Low Temperature Nuclear Transmutation forming Iron on/in Gold Electrode during Light Water Electrolysis,” *Current Topics in Electrochemistry*, **5**, pp. 37 – (1997), ISSN: 0972-4443.

[**Ohmori 1998a**] T. Ohmori, T. Mizuno, Y. Nodasaka and M. Enyo, “Transmutation in a Gold-Light Water Electrolysis System,” *Fusion Technology*, **33**, pp. 367 – 382 (1998), ISSN 0748-1896.

[**Ohmori 1998b**] T. Ohmori, T. Mizuno, K. Kurosawa and M. Enyo, “Nuclear Transmutation Reaction Occurring during the Light Water Electrolysis on Pd Electrode,” *Int. J. Soc. of Mat. Eng. for Resources*, **6** (1), pp. 35 – 44 (1998),

[**Ohmori 1998c**] T. Ohmori and T. Mizuno, “Strong Excess Energy Evolution, New Element Production and Electromagnetic Wave and/or Neutron Emission in the Light Water Electrolysis with a Tungsten Cathode,” *Proc. ICCF7*, pp. 279 – 284 (1998), ENECO Inc.

[**Ohmori 1999**] T. Ohmori and T. Mizuno, “Nuclear Transmutation Reaction Caused by Light Water Electrolysis on Tungsten Cathode under Incandescent Conditions,” *Infinite Energy*, **27**, pp. 34 – 39 (1999).

[**Ohmori 2000a**] T. Ohmori, “Recent Development in Solid State Nuclear Transmutation Occurring by the Electrolysis,” *Current Topics in Electrochemistry*, **7**, pp. 101 – 118 (2000), ISSN: 0972-4443. W, Re

- [**Ohmori 2000b**] T. Ohmori and T. Mizuno, “Nuclear Transmutation Reaction caused by the Light Water Electrolysis on Tungsten Cathode under an Incandescent Condition,” *J. New Energy*, **4-4**, pp. 66– 78 (2000), ISSN 1086-8259.W
- [**Ohmori 2002**] T. Ohmori, S. Narita, H. Yamada, T. Mizuno and Y. Aoki, “ Positive and Negative Energy Evolution and New Element Production in Critical Electrolysis with Palladium Electrode in  $K_2CO_3/H_2O$  Solution,” *Proc. JCF4*, pp. 22 – 26 (2002), ISSN 2187-2260.
- [**Ohmori 2004**] T. Ohmori, T. Mizuno, H. Yamada and S. Narita, “ Anomalous Isotopic Distribution of Palladium Generated during the Light Water Critical Electrolysis on Palladium Electrodes,” *Proc. JCF5*, pp. 36 – 40 (2004), ISSN 2187-2260.
- [**Ohmori 2016**] T. Ohmori, “Anomalous Reactions Induced by Light and Heavy Water Electrolysis”, in *New Topics in Electrochemistry Research*, Ed. M. Nunez, pp. 47 – 84, Nova science publisher, 2016, ISBN: 1-60021-015-5.
- [**Puska 1984**] M.J. Puska and R.M. Nieminen, ”Theory of Hydrogen and Helium Impurities in Metals,” *Phys. Rev.* **29B**, 5382 - 5397 (1984).
- [**Silver 1993**] D.S. Silver, J. Dash and P.S. Keefe, “Surface Topography of a Palladium Cathode after Electrolysis in Heavy Water,” *Fusion Technol.*, **24**, pp. 423 – 430 (1993), , ISSN 0748-1896.
- [**Springer 1978**] T. Springer, ”Investigation of Vibrations in Metal Hydrides by Neutron spectroscopy,” in G. Alefeld and J. Voelkl ed., *Hydrogen in Metals I*, p. 75 - 100, Springer-Verlag, Berlin, 1978.
- [**Sundaresan 1994**] R. Sundaresan and J. O’M. Bockris, “Anomalous Reactions during Arcing between Carbon Rods in Water,” *Fusion Technol.* **26**, 261 – 265 (1994), ISSN 0748-1896.
- [**Sussmann 1972**] J.A. Sussmann and Y. Weissman, ”Application of the Quantum Theory of Diffusion to H and D in Niobium,” *Phys. Stat. Sol.* **B53**, 419 - 429 (1972).
- [**Suzuki 2009**] M. Suzuki and I. Suzuki, Superexchange Interaction, (Lecture note at State University of New York at Binghamton, 2009, posted at the SUNY at Binghamton website; <http://www.binghamton.edu/physics/docs/super-exchange.pdf>
- [**Timm 2009**] Carsten Timm, Theory of Magnetism, (Lecture note at Technische Universitaet Dresden, 2009), posted at the TUD website; [https://www.physik.tu-dresden.de/~timm/personal/teaching/thmag\\_w09/lecturenotes.pdf](https://www.physik.tu-dresden.de/~timm/personal/teaching/thmag_w09/lecturenotes.pdf)
- [**Voelkl 1978**] J. Voelkl and G. Alefeld, “Diffusion of Hydrogen in Metals,” in G. Alefeld, J. Voelkl (eds.): *Hydrogen in Metals I, Basic Properties. Topics in Applied Physics*, Vol. 28 (Springer, Berlin, Heidelberg, New York 1978) pp. 321 – 348 (1978).
- [**Wicke 1978**] E. Wicke and H. Brodowsky, ”Hydrogen in Palladium and Palladium

Alloys,” in G. Alefeld and J. Voelkl ed., Hydrogen in Metals II, pp. 73 - 1558,  
Springer-Verlag, Berlin, 1978.